

The redshift evolution of early-type galaxies in COSMOS: Do massive early-type galaxies form by dry mergers?

C. Scarlata¹, C. M. Carollo¹, S.J. Lilly¹, R. Feldmann¹, P. Kampczyk¹, A. Renzini², A. Cimatti³, C. Halliday³, E. Daddi⁴, M. T. Sargent¹, A. Koekemoer⁵, N. Scoville⁶, J-P. Kneib⁷, A. Leauthaud⁷, R. Massey⁶, J. Rhodes^{6,8}, L. Tasca⁷, Capak⁶, H. J. McCracken⁹, B. Mobasher⁵, Y. Taniguchi¹⁰, D. Thompson^{6,11}, M. Ajiki¹², H. Aussel^{13,14}, T. Murayama¹², D. B. Sanders¹³, S. Sasaki^{12,15}, Y. Shioya¹⁵, M. Takahashi^{12,15}

ABSTRACT

We study the evolution since $z \sim 1$ of the rest-frame B luminosity function of the early-type galaxies (ETGs) in ~ 0.7 degrees² in the COSMOS field. In order

*Based on observations with the NASA/ESA *Hubble Space Telescope*, obtained at the Space Telescope Science Institute, which is operated by AURA Inc, under NASA contract NAS 5-26555.

¹Department of Physics, Swiss Federal Institute of Technology (ETH-Zurich), CH-8093 Zurich, Switzerland

²Dipartimento di Astronomia, Università di Padova, vicolo dell'Osservatorio 2, I-35122 Padova, Italy

³INAF- Osservatorio Astrofisico di Arcetri, Largo E. Fermi 5, I-50125 Firenze, Italy

⁴National Optical Astronomy Observatory, P.O. Box 26732, Tucson, AZ 85726

⁵Space Telescope Science Institute, 3700 SanMartin Drive, Baltimore, MD 21218

⁶California Institute of Technology, MC 105-24, 1200 East California Boulevard, Pasadena, CA 91125

⁷Laboratoire d'Astrophysique de Marseille, BP 8, Traverse du Siphon, 13376 Marseille Cedex 12, France

⁸Jet Propulsion Laboratory, Pasadena, CA 91109

⁹Institut d'Astrophysique de Paris, UMR 7095, 98 bis Boulevard Arago, 75014 Paris, France

¹⁰Subaru Telescope, National Astronomical Observatory of Japan, 650 North Aohoku Place, Hilo, HI 96720

¹¹Large Binocular Telescope Observatory, University of Arizona, 933 N. Cherry Ave., Tucson, AZ 85721

¹²Astronomical Institute, Graduate School of Science, Tohoku University, Aramaki, Aoba, Sendai 980-8578, Japan

¹³Institute for Astronomy, 2680 Woodlawn Dr., University of Hawaii, Honolulu, Hawaii, 96822

¹⁴Service d'Astrophysique, CEA/Saclay, 91191 Gif-sur-Yvette, France

¹⁵Physics Department, Graduate School of Science and Engineering, Ehime University, Japan

to identify *all* plausible progenitors of local ETGs we construct the sample of high- z galaxies using two complementary criteria: (i) A *morphological* selection based on the Zurich Estimator of Structural Types, and (ii) A *photometric* selection based on the galaxy properties in the rest-frame $(U - V)$ - M_V color-magnitude diagram. We furthermore constrain both samples so as to ensure that the selected high- z progenitors of ETGs are compatible with evolving into systems which obey a fundamental $z = 0$ scaling relation for early-type galaxies, i.e., the $\mu_B - r_{hl}$ Kormendy relation. Assuming the luminosity evolution derived from studies of the fundamental plane for high- z ETGs, our analysis shows no evidence for a decrease in the number density of the most massive ETGs out to $z \sim 0.7$: Both the morphologically- and the photometrically-selected sub-samples show no evolution in the number density of bright ($\approx L > 2.5L^*$) ETGs. Allowing for different star formation histories, and cosmic variance, we estimate a maximum decrease in the number density of massive galaxies at that redshift of $\sim 30\%$.

We observe, however, both in the photometrical and in the morphological samples, a deficit of up to $\sim 2 - 3$ of fainter early-type galaxies over the same cosmic period. Our results argue against a significant contribution of recent dissipationless “dry” mergers to the formation of the most massive early-type galaxies. We suggest that the mass growth in low luminosity ETGs can be explained with a conversion from $z \sim 0.7$ to $z = 0$ of blue, irregular and disk galaxies into low- and intermediate-mass “red”, early-type galaxies, possibly also through gas rich mergers. This interpretation is consistent with the observed increase of a factor of the order of $\sim 2 - 3$, from $z = 0$ to $z = 0.7$, of the rest-frame B -band luminosity function of blue irregular galaxies.

Subject headings: galaxies: formation — galaxies: evolution — galaxies: ellipticals — galaxies: massive spheroids — galaxies: morphologies

1. Introduction

One of the currently most debated – and consequential – issues in astrophysics is the formation of massive elliptical galaxies (see Renzini 2006, for a recent review).

From the theoretical point of view, CDM simulations can accurately predict the redshift evolution of dark matter haloes. Specifically, on large scales CDM simulations have enjoyed great success in accounting for the growth through cosmic times of the structures - clusters,

filaments and voids - starting from the extremely smooth initial conditions inferred from the cosmic microwave background (e.g. Springel, Frenk & White 2006). We still lack, however, an understanding of the astrophysical processes which produce massive galaxies with the properties that these show in the local Universe: gas cooling, star formation, stellar and AGN feedback, are all poorly -if at all- understood processes, which are currently parametrized with *ad hoc* recipes in galaxy formation models. Simulations have been less successful on these lower, galactic scales (~ 100 kpc) and it is not clear yet whether this is due to the just mentioned complexities of baryon physics, or to other reasons.

From the observational point of view, the emerging picture is still uncertain. In the local Universe, studies of the stellar populations of massive ellipticals indicate a formation epoch for the bulk of their stars at redshifts $z > 2$; however, the old stellar ages at $z = 0$ cannot break the degeneracy between the mass assembly of old smaller sub-units relative to in-situ star formation (Carollo et al. 1993; Bender et al. 1993; Carollo & Danziger 1994a,b; Bernardi et al. 2003a; Thomas et al. 2005). This degeneracy can in principle be removed by observations of the evolution of the number density of ellipticals as a function of redshift; however, small statistics, cosmic variance and details in the different analysis of the high- z samples have generated a debate as to whether massive ellipticals are already fully assembled by $z \sim 1$ – a fact which, if true, would require considerable rethinking of the currently favored galaxy formation models (see, e.g., Bell et al. 2004a, and Daddi et al. 2005 for examples of different views, and Renzini 2006 for an extensive review and further references).

Some studies have suggested that the majority of the most massive ($M > M^*$) early-type galaxies (ETGs) is assembled over the last few Gyr from the dissipationless (“dry”) mergers of less massive ETGs (Bell et al. 2004a; Faber et al. 2005). Estimates of the merger rate since $z \sim 1$ have been attempted by several authors (e.g. van Dokkum 2005; Bell et al 2006a; Lin et al. 2004; Kampczyk et al. 2006). van Dokkum (2005) used the statistics of relict tidal interactions in the local universe and conclude that $\sim 35\%$ of bulge-dominated galaxies should have experienced a merger with mass ratio $> 1:4$ since $z \sim 0.1$. Based on 6 ETG-ETG close pairs in the GEMS field, Bell et al. (2006a) estimate that each present-day ETG with $M_V < -20.5$ has undergone ~ 0.5 –2 major dry mergers since $z \sim 0.7$. Several other studies however dispute such high frequencies of dry mergers since $z \sim 1$. For example, Bell et al. (2006b), based on the 3D two-point correlation function of ETGs, conclude that only 20% of all $M > 2.5 \times 10^{10} M_\odot$ galaxies have experienced a major merger since $z = 0.8$. This result roughly agrees with the analysis of Lin and collaborators who, from the count of close pairs in the DEEP2 sample, conclude that only $\sim 9\%$ of present-day M^* galaxies have undergone a major merger over the same period. Supporting evidence against a large contribution of dry mergers to the formation of massive elliptical galaxies comes also from estimates of the dry merging rate at $z < 0.36$ from the SDSS database Masjedi et al. (2006), which show

a $< 1\%$ probability per Gyr for an ETG to merge with another ETG. The Masjedi et al. estimate implies a dry-merging rate much lower than the rate at which ETG-hosting dark matter halos merge with one another (Hogg 2006), possibly highlighting a potential problem with CDM simulations, or in the way these simulations are related to the observed galaxy populations.

In any event, there are clearly major discrepancies among current attempts at measuring the dry merger rate, which in part are the result of the uncertainty affecting the time it will take to a given galaxy pair to merge, or to some tidal debris to disappear, and in part to small-number statistics. In this paper we follow a different approach in order to set limits to the role played by dry mergers in establishing the population of massive ETGs in the local universe. Here we map the evolution with redshift up to $z \sim 0.7$ of the number density of massive ETGs. Since the bulk of stars in these galaxies formed at much higher redshifts (see the extensive literature quoted in Renzini 2006), an increase in the number density of massive ETGs since $z = 0.7$ should be ascribed to dry mergers, alternatively, a lack of evidence for such an increase would allow us to set limits on the dry merging rate.

We use the data from the COSMOS program (Scoville et al. 2007a) to study the evolution of the luminosity function (LF) of the ETGs up to redshift $z = 1$. We base the analysis on the sample of $\sim 32,000$, $I_{AB} \leq 24$ COSMOS galaxies with reliable photometric redshift in the range $0.2 < z \leq 1.0$ presented in Scarlata et al. (2007, hereafter Paper I) to extract a combined sample of 3980 morphologically- and/or photometrically-selected progenitors of early-type systems to study, in the $z = 0$ to $z = 1$ redshift window, their LF evolution in the rest-frame B -band. Specifically, we select two complementary samples of possible progenitors of massive ETGs, and study their individual and combined redshift evolution. The first sample is selected morphologically, using the classification of ZEST (Zurich Estimator of Structural Types, Paper I). The second sample is selected photometrically, using the red-sequence identified, at all redshifts, on the rest-frame $(U - V) - M_V$ diagram. Both samples are further constrained by requiring that, by passive-evolution fading, the high- z progenitors of ETGs evolve into $z = 0$ systems that lie on the $\mu_B - r_{hl}$ “Kormendy relation” (Kormendy 1977).

Our double (i.e., morphological and photometrical) selection is motivated by the fact that, at $z = 0$, elliptical galaxies are characterized by well defined stellar population and dynamical/structural properties. Specifically, $z = 0$ ellipticals *both* (a) Have uniformly-old stellar populations with a small scatter in the observed colors, implying a small scatter in the formation epoch of their stellar populations; *and* (b) Are described by regular surface brightness distributions, well represented by almost deVaucouleurs density profiles, indicating a large role of violent relaxation in their dynamical history. Depending on the relative

timing and importance of in-situ star formation versus stellar mergers, $z \sim 1$ progenitors of ellipticals may thus appear as already morphologically-relaxed systems or possibly show passively-evolving stellar populations with irregular morphologies due to recent mergers. Therefore, to identify *all* plausible high- z progenitors of local ETGs we consider the sample created by the union of the morphologically and photometrically selected galaxies. This sample allows us to be comprehensive in the “counting” of the number density of massive galaxies at earlier epochs. Still, selection biases remain in our analysis: The photometrically-selected sample could include galaxies which are actually not progenitors of ellipticals and have red colors simply because of the effects dust extinction. On the other hand, blue progenitors with merger morphologies would not enter in either of the samples. We discuss later in the paper the impact of these biases on our conclusions.

The paper is organized as follows. Section 2 describes the data and the basic measurements; Section 3 describes in detail the sample selection criteria; Section 4 quickly summarizes the structural properties of the photometrically-selected ETGs, and the color properties of the morphologically-selected sample; Section 5 presents our main analysis, i.e., the evolution with redshift of the rest-frame B -band LF of the different and also combined samples of high- z ETG progenitors. We discuss our results in Section 6 and highlight a few concluding remarks in Section 7. Appendix A presents the tests performed on the LFs to account for the photometric redshift uncertainties, and Appendix B presents the SDSS-based $z = 0$ comparison sample. Throughout the paper we assume $\Omega_m = 0.25$, $\Omega_m + \Omega_\Lambda = 1$, and $H_0 = 70$ km s⁻¹ Mpc⁻¹. All magnitudes are AB magnitudes (Oke 1974), unless otherwise specified.

2. Data and basic measurements

2.1. The data and the input catalogue

The analysis presented in this paper uses the COSMOS Hubble Space Telescope (HST) Advanced Camera for Survey (ACS) F814W images (hereafter I_{AB}), and ancillary ground-based UV to near-infrared data available for the COSMOS field. The ground-based B_J , g^+ , V_J , r^+ , i^+ , z^+ data were acquired with the Subaru Telescope, the u^* -band data with the Canada–France–Hawaii Telescope, and the infrared K_S images with the Cerro Tololo International Observatory and Kitt Peak National Observatory telescopes. The observations and the data processing are described in detail in Capak et al. (2007), Taniguchi et al. (2007), for the ground-based data; and in Koekemoer et al. (2007) for the HST-ACS data.

Photometric catalogs were created separately for the ground-based and the HST data. The ACS-based catalog was generated by Leauthaud et al. (2007) using SExtractor (Bertin & Arnouts

1996) in a two steps strategy, in order to correctly detect and deblend objects with a wide range of magnitudes and sizes. Extensive simulations presented in Leauthaud et al. (2007) show that the ACS catalog is at least 90% complete for objects smaller than $1''.4$ and $I_{AB} \leq 24$ (roughly corresponding to a surface brightness limit of $\mu_{I_{AB}} = 25 \text{ mag arcsec}^{-2}$).

The ground-based catalog was generated using SExtractor in dual-image mode. The detection was performed in the original best-seeing PSF i^+ -band image, while the photometry was measured in the PSF-matched images. This process ensured that the photometry of nearby galaxies was optimally deblended in the final catalog. Magnitudes were measured within apertures of $3''$ diameter; and 5σ magnitude limits are 26.4, 27.3, 27.0, 26.6, 26.8, 26.2, 25.2, and 21.6 in the u^* , B_J , g^+ , V_J , r^+ , i^+ , z^+ , and K_S filters, respectively (Capak et al. 2007).

In this work, we present the results for the central area of the COSMOS field of ~ 0.74 degrees² covered by the 260 ACS pointings acquired during HST Cycle 12 observations. We limit our study to the $\sim 32,000$ galaxies with total magnitude (as measured by the SExtractor MAG_AUTO) brighter than $I_{AB} = 24.0$ and photometric redshifts (see next Section) in the redshift range $0.2 < z \leq 1.0$.

2.2. Photometric redshifts

We adopt the Maximum Likelihood photometric redshift estimates obtained for the COSMOS galaxies by Feldmann et al. (2006) with the Zurich Extragalactic Bayesian Redshift Analyzer (ZEBRA). Our photo- z were obtained using as a basic set of galaxy templates the empirical spectra by Coleman, Wu, & Weedman (1980) and Kinney et al. (1996), that cover the spectral types from elliptical to the star-forming galaxies. By means of an iterative technique ZEBRA automatically corrects their original set of templates to best represent the galaxy spectral energy distributions (SEDs) in different redshift bins (to empirically take into account, e.g., dust absorption effects and other possible inadequacies inherent in the original set of templates). The availability of a “training set” of spectroscopically-derived z -COSMOS redshifts (Lilly et al. 2007) for a small fraction of the whole photometric sample under investigation allows ZEBRA to achieve an optimal correction of the galaxy templates and a precise calibration of the photometric redshifts, and thus accurate photo- z estimates.

The resulting photometric redshifts have an accuracy of $\sigma_z/(1+z) = 0.027$ over the whole redshift range considered in the current analysis, relative to the z COSMOS spectroscopic redshifts of $I_{AB} \leq 22.5$ galaxies. Tests on the $I_{AB} \leq 22.5$ spectroscopic sample artificially fainted to reproduce a $I_{AB} \leq 24$ sample, indicate photometric redshift errors $\sigma_z/(1+z) \sim$

0.06.

We checked that our main results remain unchanged when: (a) changing the redshift binning adopted by ZEBRA for the template optimization, the minimum errors in the photometry allowed by ZEBRA, the corrections applied to the photometric catalog (i.e., the plianthness parameter $-\sigma-$ and the regularization parameter $-\rho-$, that appear in the χ^2 minimization approach of the ZEBRA code; Feldman et al. 2006); (b) using only galaxies with $\chi^2 < \chi_{95}^2$ in the ZEBRA fits, with χ_{95}^2 the value corresponding to the 95th percentile in an ideal χ^2 -distribution of a varying number of degrees of freedom; or all galaxies in the sample, independent of their χ^2 in the ZEBRA photometric fits.

For a total of $\sim 4.4\%$ of the galaxies that were detected in the original ACS-based catalogue it was not possible to derive photometric redshift estimate, due to either their absence, or their blending with other galaxies in the ground-based catalogue. These galaxies were excluded from our analysis. The usable Cycle 12 $I_{AB} \leq 24$ ACS-based catalogue contains 32540 galaxies with photometric redshift in the range $[0.2, 1.0]$ and $\chi^2 < \chi_{95}^2$.

2.3. The ZEST morphological classification

To extract the sample of *morphologically-selected* ETGs at high redshifts, and also to study later on in the paper the morphologies of the photometrically-selected sample of ETGs, we used the ZEST classification presented in Paper I.

ZEST quantitatively describes the galaxy structure using three variables (PC_1 ; PC_2 ; PC_3), obtained by performing a principal component analysis (PCA) in the five-dimensional parameter space of asymmetry (A), concentration (C), Gini coefficient (G), the 2nd-order moment of the brightest 20% galaxy pixels (M_{20} , e.g., Abraham et al. 2003; Lotz, Primack & Madau 2004), and the ellipticity of the light distribution¹ (ϵ). These non-parametric diagnostics provide complementary, but also redundant information on galaxy structure. With the PCA we found that the first three PC variables explain more than 90% of the variance in the original dataset, and thus completely describe the galaxy structure.

The morphological classification is performed in the space with axes $PC_1 - PC_2 - PC_3$. To associate a (dominant) morphological class to different regions in the PC -space, the latter was partitioned into a regular 3D-grid with unit steps in each of the coordinates, and

¹In order to ensure a meaningful comparison of the parameters among galaxies at different redshifts, all coefficients are computed within elliptical apertures of semi-major axis equal to one Petrosian radius (Petrosian 1976)

all the galaxies in the COSMOS sample within each of the unit PC -cubes were visually inspected. Each galaxy was then assigned the morphological class of the PC -cube corresponding to its position. The ZEST classification associates to each PC -cube a Type ($= 1$ for early-type galaxies; $= 2$ for disk galaxies; and $= 3$ for irregular galaxies). Furthermore, each PC -cube classified as Type 2 is assigned a “bulgeness” parameter according to the median value (n_m) of the distribution of n Sersic indices of all galaxies brighter than $I_{AB} = 22.5$ in that cube. The two-dimensional GIM2D fits were performed by Sargent et al. (2007) on the COSMOS-bright sample, i.e., $I_{AB} \leq 22.5$; we verified in Paper I that the PCA provides consistent results if separately applied to the faint (i.e., $I_{AB} \leq 24$) and the bright (i.e., $I_{AB} \leq 22.5$) samples. The “bulgeness” parameter is related to the B/D ratio ² (see Paper I for detail) and ranges from 0 (bulge dominated disk galaxies, Type 2.0) to 3 (pure disk galaxies, Type 2.3). We use n_m to assign the bulgeness parameter to each Type 2-classified PC -cube, according to the following scheme: bulgeness = 3, 2, 1, and 0 respectively for $0 < n_m < 0.75$, $0.75 \leq n_m < 1.25$, $1.25 \leq n_m < 2.5$, and $n_m \geq 2.5$. The distributions of Sersic n for all galaxies classified as Type 2, splitted according to their bulgeness parameter are shown in Figure 9 of Sargent et al. (2007).

In Paper I we discuss in detail the uncertainties and the systematic errors in the measured structural parameters as a function of signal-to-noise ratio (S/N), and to what extent the COSMOS-calibrated ZEST morphological classification grid is affected by the S/N of the individual galaxies; our tests show that the ZEST morphological classification is robust down to $I_{AB} = 24$. Furthermore, the ZEST classification is substantially more efficient in disentangling different galactic types than simpler classification schemes based on, e.g., a threshold in n -Sersic index, or two/three of the non-parametric diagnostics mentioned above.

2.4. Rest-frame magnitudes and colors

In order to compute the rest-frame absolute B -band magnitude (M_B), we define a color k -correction $K_{BI}(z) = B - I_z$, where B is the magnitude at $\lambda_{B,\text{obs}} = (1 + z) \times \lambda_B$, and I_z indicates the observed I -band magnitude for a galaxy at redshift z . The central wavelength of the ACS filter (F814W) corresponds to the central wavelength of the B -band at redshift $z \sim 0.8$, therefore $B - I_{z \sim 0.8} = 0$. It follows that the rest-frame absolute magnitude M_B can be expressed as:

²When single Sersic fits are performed to bulge+disk galaxies, the n Sersic index of the *global* galaxy profile is found to be monotonically related to the galaxy B/D ratio (e.g., Blanton et al. 2003).

$$M_B = I_z - 5.0 \log(d_L(z)/10\text{pc}) - 25.0 + K_{BI}(z) + 2.5 \log(1 + z), \quad (1)$$

where d_L is the luminosity distance at redshift z . The color $B - I_z$ depends on the galaxy spectral energy distribution. For each galaxy we therefore use its ZEBRA best-fit template and the corresponding photometric redshift to compute the $B - I_z$ color.

The rest-frame $U - V$ colors are derived from the ground-based photometry, by interpolating the observed SEDs at the wavelengths of the U and V filters, redshifted at the galaxy photometric redshift. The adopted effective wavelengths of the U and V filters are 3841 Å, and 5479 Å, respectively. Typical accuracy in the rest-frame $U - V$ color is of 0.05 mag for $\sigma_z \sim 0.03(1 + z)$, and 0.1 for $\sigma_z \sim 0.06(1 + z)$.

3. Selection of high- z progenitors of early-type galaxies

3.1. The morphologically-selected sample

The morphologically-selected sample was constructed by including all galaxies classified by ZEST as Type 1, i.e., as early-type galaxies, and all bulge-dominated Type 2.0 disk galaxies. The latter are located in volumes of PC -space that are adjacent to the Type 1 early-type galaxies, and are therefore characterized by very similar structural properties (see Paper I). Indeed, Type 2.0 galaxies have bulge properties very similar to the Type 1 systems, and differ from these only for a clearly detected (non-dominant) disk component. Down to the magnitude limit of our analysis ($I_{AB} = 24$), in the fraction of the COSMOS field under investigation, and in the redshift range $0.2 < z \leq 1.0$ there are a total of 2352 and 1352 galaxies, with good photometric redshift that are respectively classified as Type 1 and Type 2.0 galaxies by ZEST. Both samples have similar Sersic n distribution, with 80% and 70% of Type 1 early-type and Type 2.0 bulge dominated galaxies, respectively, having $n \geq 2.5$. We highlight in the Sections below further similarities between Type 1 and Type 2.0 galaxies. The inclusion of these (heavily) bulge-dominated disk galaxies in our morphologically-selected sample of ETGs also facilitates the comparison with other studies, since these have generally tended to include such systems in the analysis (see, e.g., Bell et al. 2004b).

3.1.1. A further constraint: The $z=0$ Kormendy relation

ETGs in the local universe follow well defined scaling relations. Of particular importance is the fundamental plane (Djorgovski & Davis 1987; Dressler et al. 1998) and, if the velocity dispersion is not available, its photometric projection, i.e., the so-called “Kormendy-relation” (Kormendy 1977). The Kormendy relation is a correlation between the half–light radius of the galaxy and the average surface brightness within the half–light radius.

Selecting ETG progenitors at high redshifts on the basis of their elliptical-like morphologies is equivalent to requiring that these progenitors are already fully assembled and dynamically-relaxed galaxies at those earlier epochs: they become $z = 0$ early-types by evolution of their stellar populations (and possibly some modest amount of additional star formation). Therefore, in constructing a morphologically-selected sample of high- z ETGs, we can apply an additional constraint, namely the surface brightness must be such that with plausible surface brightness evolution it evolves in to the Kormendy relation. Clearly, surface brightness evolution may be uncertain, especially for blue objects with composite stellar population, however we can take a conservative approach and estimate a minimum evolution that leads to the minimum number of excluded objects.

In Figure 1 we show the average surface brightness within the half–light radius in the rest-frame B –band as a function of the half–light radius for the Type 1 (early-type galaxies, left panel) and Type 2.0 (bulge-dominated disk galaxies, right panel) galaxies of our morphologically-selected sample. We use different colors to represent galaxies with different ZEBRA best–fit to their SEDs; in particular, red points are galaxies fitted by ZEBRA with an “elliptical-galaxy” template, and blue points represent later spectral types (Feldmann et al. 2006). Dotted and dot-dashed lines show the $I_{AB} = 24$ magnitude limit at the central redshift of the bin, for galaxies with the SED of a star-forming and an elliptical galaxy, respectively. Typical error-bars (i.e., estimated at the median size and magnitude of the sample galaxies) are shown on the upper right part of each panel. The errors are calculated by also taking into account the effects of the photometric redshift. The half-light radii used in Figure 1 are measured using a growth curve analysis on the ACS I_{AB} images. By comparison with the half-light radii measured with GIM2D by Sargent et al. (2007) we found that PSF effects; which are accounted for with GIM2D, start to be important only for galaxies with measured $r_{hl} < 0''.2$. At these sizes, r_{hl} is typically overestimated by $\sim 25\%$ compared with the GIM2D measurement. We find similar results by analyzing a set of $I_{AB} = 22 - 24$ simulated galaxies with Sersic index $n = 2$, and 4. We decided not to correct for this effect, since the correction depends on the exact shape of the galaxy surface-brightness profile, which is unknown. We note, however, that our sample includes only $\sim 7\%$ of galaxies with measured $r_{hl} < 0''.2$, so the impact of the PSF correction on the final selected sample of Kormendy-consistent

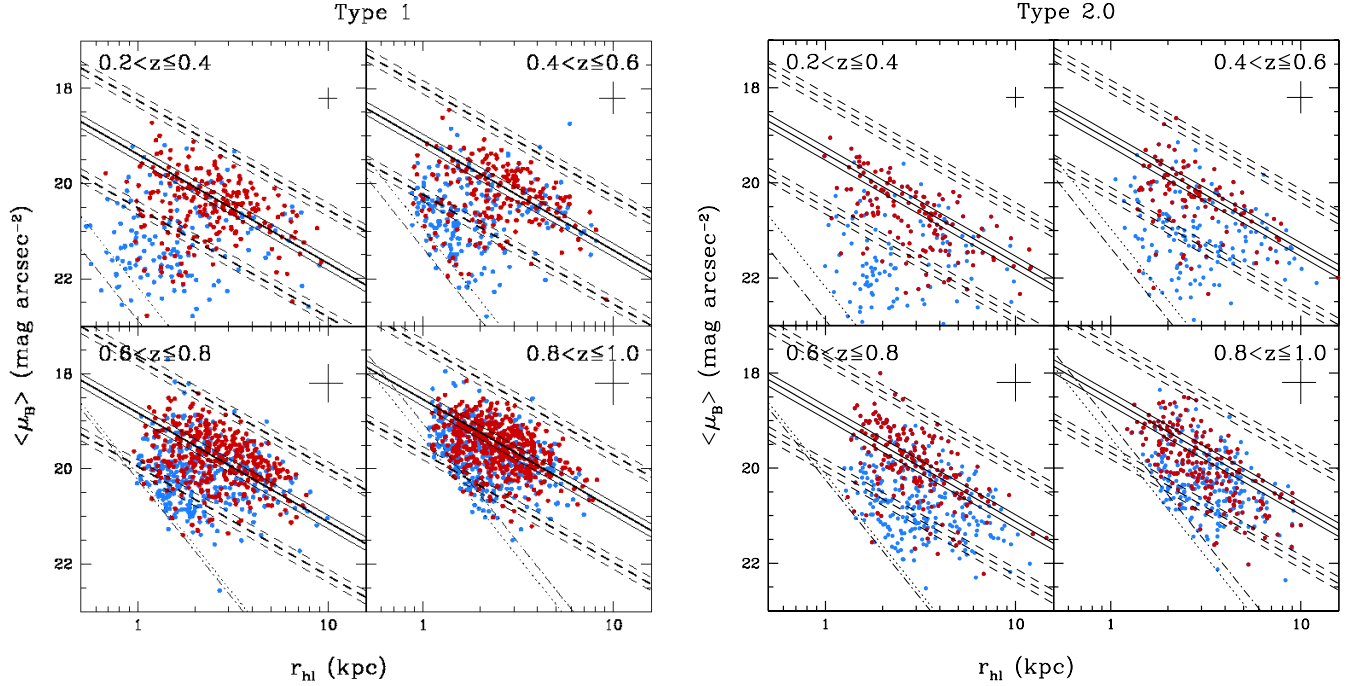


Fig. 1.— Average surface brightness within the half-light radius in the rest-frame B -band ($\langle \mu_B \rangle$) as a function of the half-light radius (r_{hl} , in kpc) for all galaxies *morphologically*-classified as early-type galaxies (ZEST Type 1; left) and bulge-dominated disk galaxies (ZEST Type 2.0; right). In each Figure, the four panels correspond to different redshift bins, as indicated. Points are color-coded according to the best-fit ZEBRA spectral types: red points correspond to galaxies with ZEBRA elliptical-galaxy SED, and blue points represent all galaxies with later ZEBRA spectral types. The solid black line represents the best linear fit derived for the $z = 0$ Coma cluster galaxies (Jørgensen, Franx & Kjærgaard 1995), passively evolved at the central redshift of the considered bin. The solid thin lines represent the evolution of the best-fit relation at the extremes of the redshift bin. The dashed lines indicate a distance from the best-fit line of twice the rms of the $z = 0$ relation. Dotted and dot-dashed lines show, at the central redshift of bin, the $I_{AB} = 24$ magnitude limit for galaxies with the SED of a star-forming and an elliptical galaxy, respectively. On the upper right of each panel we show the typical error bar in $\langle \mu_B \rangle$ and r_{hl} .

galaxies is minimal. In the Figure, the solid black line represents the best linear fit derived for the Coma cluster galaxies (Jørgensen, Franx & Kjørgaard 1996), passively evolved at the central redshift of the bin assuming $\mu_B(z) \propto -1.36z$ [i.e., the evolution of a single stellar population model with formation redshift $z_f = 2$; Bruzual & Charlot (2003)]. The Jørgensen et al. (1995) data were converted from Johnson VEGA to AB magnitudes using the relation $B_{AB} = B_{VEGA} - 0.1$. The solid thin lines represent the best fit relation at the two extremes of the redshift bins. The dashed lines indicate a distance from the $z = 0$ best fit line of twice its rms dispersion.

Figure 1 shows that up to redshift $z \sim 1$, for a given size, objects that have a ZEBRA elliptical-like classification tend to have, on average, higher surface brightness relative to those with later spectral types. Furthermore, the Figure shows that, up to $z \sim 0.6$, many galaxies lie significantly below the local Kormendy relation. A Fraction of order $\sim 80\%$ of these “low-density” systems have the ZEBRA SEDs of late-type, star-forming galaxies. We note that at redshifts higher than $z = 0.6$ selection effects are responsible for the absence of galaxies with $\langle \mu_B \rangle \sim 22$ mag arcsec $^{-2}$ and radii of few kiloparsecs.

In order to quantify the criterion for the exclusion of implausible progenitors of ETGs on the basis of the $z = 0$ Kormendy relation, we followed the procedure described in Ferreras et al. (2005), namely:

- We assigned a fading rate of μ_B to each galaxy, based on the ZEBRA best fit to its SED.
- We considered two extreme star formation histories (SFHs), both with an initial formation redshift $z_f = 2$. The first SFH describes the passive evolution of a single burst stellar population and was assigned to all galaxies with a ZEBRA “elliptical galaxy” best-fit. The second SFH was assigned to galaxies best fitted by ZEBRA with a star-forming SED. This SFH is described by a constant star formation rate of $1M_{\odot}/\text{yr}$ up to the redshift at which the galaxy is observed (if larger than $z = 0.5$), and by zero SFR from the galaxy redshift (or $z = 0.5$) to $z = 0$. The lowest redshift possible for the truncation of the star formation, i.e., $z = 0.5$, was chosen in order for the $z = 0$ stellar population of the so-evolved galaxies to have colors consistent with the observed scatter in the color–magnitude relation of nearby ETGs (Bower, Lucey, & Ellis 1992; Bernardi et al. 2003a). The SFHs, i.e., the μ_B fading rates, for intermediate ZEBRA photometric types were derived by interpolating between the two extreme cases. The evolution of the SFHs was computed assuming a constant metallicity equal to the solar value.
- Finally, we excluded from the final sample of “Kormendy-compatible”, morphologically-

selected progenitors of ETGs all objects that, when evolved to $z = 0$ with the above evolutionary tracks, were found to lie away from the local Kormendy relation³ at a distance more than 2 times its observed scatter. Using a threshold of 3 times the observed scatter would increase the number of galaxies included in the final sample of Kormendy-compatible ETGs by $\lesssim 10\%$, without changing our main conclusions on the evolution of the number density of bright ETGs.

This selection might in principle be affected by the specific value of the adopted formation redshift ($z_f = 2$) and the approach of using the ZEBRA best fit templates to determine the B -band surface brightness evolution of each galaxy. However, neither of these choices affects our final conclusions.

First, if some of the galaxies which have a ZEBRA elliptical-galaxy fit were actually reddened star-forming objects, then the number of rejected objects would be minimized.

Assuming a slower B -band luminosity evolution (i.e., a higher formation redshift of, e.g., $z_f = 3$) would change the expected brightening at redshift $z = 1$ by ~ 0.2 magnitudes, resulting in a final sample of kormendy-consistent ETGs only $\sim 7\%$ larger than the sample obtained using $z_f = 2$. Our choice of using $z_f = 2$ is supported by recent results, based on the evolution of the fundamental-plane, showing that $M > 10^{11} M_\odot$ early-type galaxies have $z_f = 2.01_{-0.17}^{+0.22}$ (van Dokkum & van der Marel 2006), with no significant differences for ETGs in cluster and field environment. Although z_f measured by van Dokkum & van der Marel (2006) is a luminosity weighted mean star-formation epoch, the star-formation timescale for massive ETGs, estimated from $z = 0$ ellipticals, is shorter than 1 Gyr. Furthermore, Dickinson et al. (2003) and Papovich et al. (2006) show that the star formation in massive galaxies is largely completed by $z \sim 1.5$. Although the evolution of the stellar-population for less massive ETGs is less constrained, there is evidence that less massive ETGs evolve faster than high mass ones, both in the field and in cluster (McIntosh et al. 2005; Treu et al. 2005). In the light of our results a mass independent formation redshift is thus a conservative approach, since it gives the smallest number of rejected low luminosity ETGs.

The Kormendy-cut increases the fraction of galaxies in the morphologically-selected (Type 1+2.0) sample which also have the ZEBRA SED of an elliptical galaxy: this increases from 53% to 63%. Particularly affected are the lowest redshift bins up to $z = 0.6$, in which the fraction of early-type morphologies with an early-type SED increases from 53% to 70%.

³The $z = 0$ Kormendy-relation, as we discussed in the text, is derived using galaxies belonging to the Coma cluster. Bernardi et al. (2003b) -see also discussion in Renzini (2006)- found that there are very small differences in the fundamental plane derived for galaxies in cluster or in the field, and these differences remain small up to redshift ~ 1 (van Dokkum & van der Marel 2006).

We note that about 46% of the excluded ZEBRA late-type galaxies at redshifts $z < 0.6$ are faint systems with $I_{AB} \geq 23$. In the highest redshift bin, the fraction of excluded objects with ZEBRA late-type SEDs reduces to 20%, and only 1% of the ZEBRA elliptical type objects do not pass the Kormendy-relation test.

A similar fraction of Type 1 and Type 2.0 galaxies are excluded on the basis of the Kormendy relation constraint: the fraction of Type 2.0 galaxies in the final morphologically-selected sample changes from 37% to 35% before and after the Kormendy-cut, i.e., it remains basically constant. The exclusion of the “Kormendy-rejected” objects implies a cut of about 20% in the original sample of ZEST morphologically-selected early-type galaxies: Our *final sample of morphologically-selected* progenitors of ETGs contains 2730 galaxies (1798 Type 1 and 932 Type 2.0 systems).

3.2. The photometrically-selected sample

Progenitors of $z = 0$ massive ETGs may appear, at $z \sim 1$, as morphologically-irregular, merging systems with old and passively evolving stellar populations. These galaxies can be selected on the basis of their SED properties.

To define our COSMOS sample of photometrically-selected progenitors of $z = 0$ ETGs, we used the red-sequence identified on the rest-frame $(U - V)$ - M_V color-magnitude diagram, as derived in the two-step procedure that we describe below.

3.2.1. Step 1: Identification of the “initial red sequence”

In the left panel of Figure 2 we show the rest-frame $(U - V) - M_V$ color-magnitude diagram for the COSMOS $I_{AB} \leq 24$ galaxy sample, split in four redshift bins. The grey levels in each panel represent the weighted galaxy volume density in bins of 0.15 of M_V magnitude and 0.04 of $U - V$ color; the density in each color-magnitude bin is computed as $\sum_i W_i / V_{max,i}$. The $V_{max,i}$ value is the maximum volume within which a galaxy i , with a given observed I_{AB} magnitude and spectral type, is detectable in the COSMOS survey; the weights W_i are the corrections required so as to account for objects excluded either because no redshift is available, or because the redshift estimate is less accurate than the required threshold (see Section 2.2, and also Paper I for details on the derivation of the W_i values). The grey scale bar at the top of each panel shows the density in Mpc^{-3} corresponding to the grey intensity levels.

The presence of radial color gradients in galaxies can have an effect on the measured

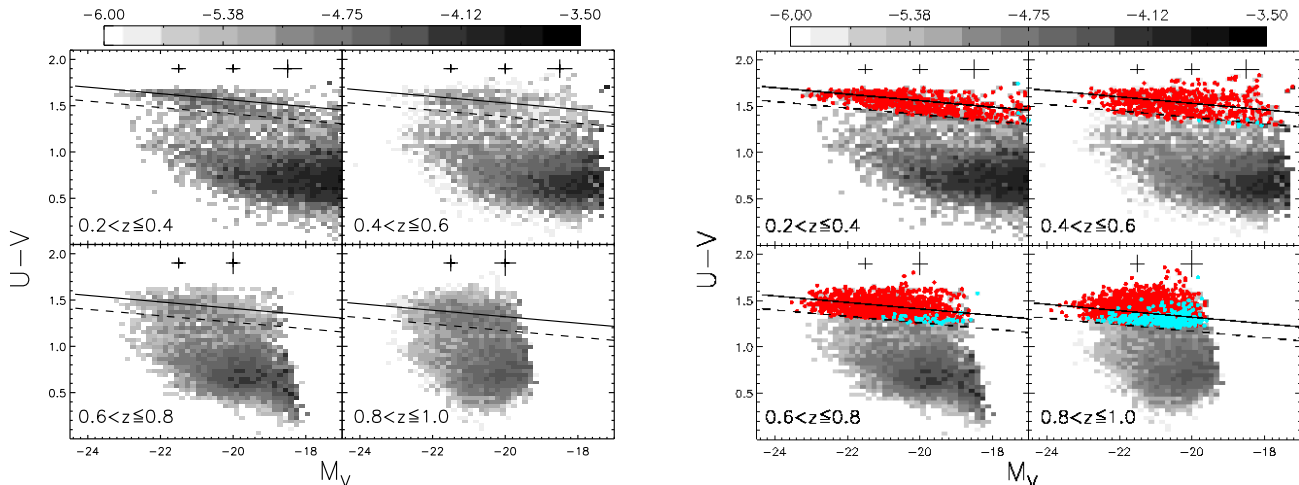


Fig. 2.— Left panel: Rest-frame $U - V$ color versus absolute magnitude in the rest-frame V -band, for the same redshift bins as in Figure 1. In each redshift bin, the solid lines represent the color-magnitude relation of the red sequence at the central redshift of the bin (Section 3.2.1); dashed lines are $-3 \times \text{rms}$ away from the solid lines. The grey levels represent the weighted volume density of galaxies in bins of 0.06 of $U - V$ color and 0.15 of magnitude, as indicated by the grey-scale shading bar given on top of each panel. Right panel: Same rest-frame color magnitude diagrams as in the left panel, with highlighted in red and blue the galaxies belonging to the photometrically-selected sample. In this panel, red points indicate galaxies with a ZEBRA SED best fit of an elliptical-galaxy, and blue points are galaxies which belong to the photometrically-selected sample but have later spectral types according to the ZEBRA fits.

colors and on the slope of the red sequence, depending on the size of apertures used to compute colors and magnitudes (see, e.g. Scodreggio 2001). Although not easy to quantify, an estimate of this effect can be evaluated as follows. The galaxy colors in the COSMOS photometric catalogue are computed within $3''$ diameter apertures, regardless of galaxy redshift (Capak et al. 2007). The local magnitude-size relation implies a half-light radius of ~ 6 kpc at $M_B \sim -21.5$ and of ~ 2 kpc at $M_B \sim -19.5$; therefore, when no evolution is taken into account, the COSMOS $3''$ aperture correspond to ~ 1.2 and ~ 3.4 half-light radii for bright and faint galaxies, respectively. Assuming a De Vaucouleur profile and using the average $U - V$ color gradient derived by Scodreggio (2001; $d(U - V)/d(\log R) = -0.15$), the $U - V$ colors computed within 1.5, 2.0, 2.5, and 5 r_{hl} differ from the color computed within 0.3 r_{hl} respectively by ~ -0.05 , -0.07 , -0.08 , -0.11 magnitudes. Given the assumptions on the shape of the galaxy surface-brightness profile, on the value for the local color-gradient, and on the size-luminosity relation, the estimates of the effect of the color gradient on the

measured colors can only be considered as indicative, and we therefore decided not to correct the data, but rather to consistently derive the slope of the red sequence from the observed COSMOS color-magnitude diagram in each redshift bin.

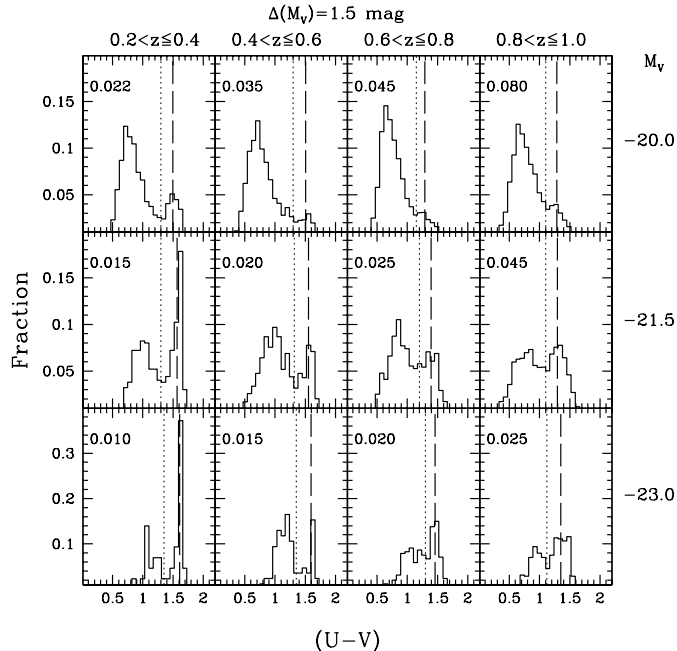


Fig. 3.— Distribution of the rest-frame $U - V$ color for the COSMOS galaxies. We divide all galaxies in four redshift bins (one redshift per column) and three magnitude bins of 1.5 magnitudes for each redshift (as indicated on the right side of the plot). The number in the upper-left corner of each panel indicates the median error on the $U - V$ colors in each magnitude–redshift bin (Section 3.2.1). The dotted vertical line shows the $(U - V)_{irs}$ color that we use to broadly isolate the red sequence in each redshift–magnitude bin; the color of the peak in each bin ($(U - V)_{redpeak}$) is indicated by the vertical dashed line. The histograms are normalized to the total number of objects in each magnitude–redshift bin.

In Figure 3 we show the normalized distribution of the rest-frame $U - V$ color of all galaxies split in both redshift and absolute magnitude. In particular, we consider four redshift bins, one per column, and three bins of 1.5 magnitudes centered at the values indicated in the Figure (top: $M_V = -20$; middle: $M_V = -21.5$; bottom: $M_V = -23$). All panels in the Figure show a degree of bimodality between red and blue galaxies (see e.g., Bell et al. 2004a, for a discussion of color bimodality at high redshift), albeit with varying degrees of sharpness. We are nonetheless able to identify in each of the panels the color of the “red peak”, which we use as the starting point for the computation of the slope of the red sequence in each of the individual redshift bins.

Specifically, in each magnitude–redshift bin, we define $(U - V)_{irs}$ as the color which broadly isolates the *initial red sequence*; $(U - V)_{irs}$ is defined as the color of the minimum in the valley between the blue and red peak in each of the color distributions, and it is indicated as a dotted line in each panel of Figure 3. The $(U - V)_{redpeak}$ color is then computed as the median of all colors redder than $(U - V)_{irs}$. The $(U - V)_{redpeak}$ color is indicated with a black dashed vertical line in each panel of Figure 3. The number in the upper-left corner of each panel indicates the median error on the $(U - V)_{redpeak}$ colors in each magnitude–redshift bin; in some bins, these are negligible. These median errors are conservatively obtained considering the maximum error derived by interpolating the errors in each of the two adjacent passbands that are used to derive the rest-frame $(U - V)$ color of the galaxy. We tested that varying the adopted color thresholds (i.e., $(U - V)_{redpeak}$) within $\pm 3\sigma_{(U-V)}$ does not affect the resulting sample of photometrically selected ETGs.

We then compute the slope of the *initial red sequence* in each redshift bin by fitting a linear relation to the $M_V - (U - V)_{redpeak}$ points (and their errors). The four slopes, as a function of increasing redshift, are: -0.037 ± 0.007 , -0.032 ± 0.011 , -0.040 ± 0.015 , and -0.029 ± 0.020 . Within the errors, these values are consistent with the average of -0.035 ± 0.005 . Given the measured uncertainties, we therefore choose to keep fixed in our analysis the average slope of the red-sequence to the “consistency value” of $-0.035(\pm 0.005)$ for all redshifts.

For each galaxy in each redshift bin, a “slope-corrected” color is then obtained by setting $(U - V)_{corr} = (U - V) + 0.035 M_V$. The zero point of the initial red sequence at the mean redshift of each bin is thus defined as the color of the red peak of the $(U - V)_{corr}$ distributions. These zero point colors $(U - V)_{ZP}$ are equal to 0.86 ± 0.04 , 0.83 ± 0.05 , 0.71 ± 0.06 , and 0.62 ± 0.05 at the redshift values corresponding to the center of our bins, i.e., $z = 0.3, 0.5, 0.7$, and 0.9 , respectively. The error-bars are computed by estimating the shifts in the red peak of the $(U - V)_{corr}$ distributions induced by a change in the red-sequence slope of $\pm 1\sigma$.

The above-defined initial red-sequence curves are shown, for each redshift bin, as solid lines in the left panel Figure 2; in each panel, the dashed line is -3σ away from the initial red sequence.

3.2.2. Step 2: Refining the red-sequence: The final photometrically-selected sample

The initial red sequence derived above coarsely mixes galaxies within broad redshift bins. To refine the evolution with redshift of the zero point, we plot in Figure 4 the values

of $(U - V)_{ZP}$ derived above as a function of redshift. Specifically, Figure 4 shows the rest-frame $U - V$ color as a function of redshift for an absolute V magnitude of -20.0 , passively evolved by assuming a single burst stellar population formed at redshift $z_f = 2$ and metallicity $Z = 0.8Z_\odot$. The color evolution of the model is shown in Figure 4 as a dashed line.

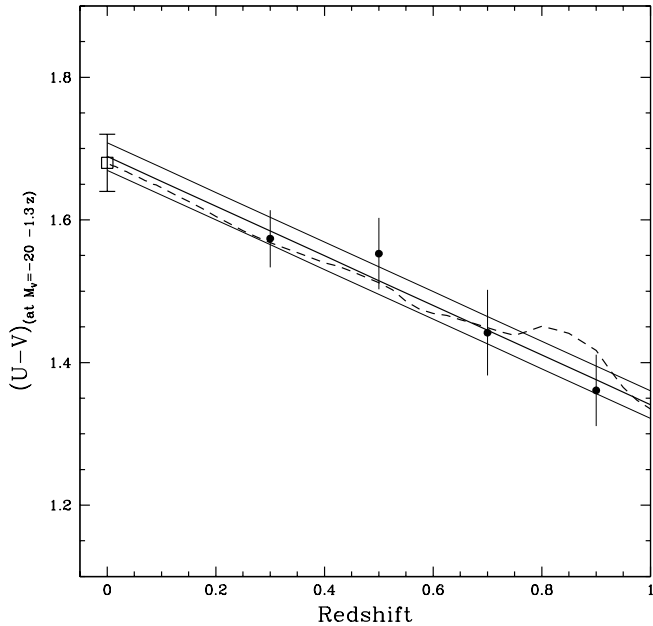


Fig. 4.— The circles represent the $U - V$ color of the initial red sequence calculated, as a function of redshift, at a magnitude $M_V = -20.0$ passively evolved using a single-burst stellar population with formation redshift $z_f = 2$ and metallicity $Z = 0.8Z_\odot$. The color evolution of this model is shown as a dashed line. The error bars are those listed for the $(U - V)_{ZP}$ in Section 3.2.2. The $z = 0$ point is derived applying the same procedure adopted for the COSMOS galaxies to the comparison SDSS sample. The thick solid line shows the linear fit to the color evolution of the zero point of the red sequence, derived including the SDSS comparison data point. The thin solid lines are $1\ rms$ away from the best fit.

The $z = 0$ point shown in Figure 4 is obtained by applying to the comparison SDSS sample described in Appendix B (and discussed in detail in Kampczyk et al. 2007), the same procedure that we have described above for the COSMOS galaxies. The observed redshift evolution of the $U - V$ color of the red-sequence at $M_V = -20 - 1.3z$ is consistent with the evolution predicted for the single stellar population formed at redshift $z_f = 2$, that also reproduces the $z = 0$ $U - V$ color of the red-sequence of the SDSS ETG sample.

A linear fit in the $0 \leq z \leq 1$ redshift range (i.e., including the SDSS point) to the $(U - V)_{ZP}$ - z relationship at the evolved $M_V = -20$ magnitude gives:

$$(U - V)_{ZP} = (-0.37 \pm 0.04) z + (1.69 \pm 0.02). \quad (2)$$

This best fit is shown in Figure 4 as a thick solid line; thin solid lines are located 1 *rms* away from the best fit. This result is in agreement with the redshift evolution of $(U - V)_{ZP}$ found by Bell et al. (2004a). We use this best fit, together with the slopes measured as described in Section 3.2.1, to define the final red sequence at any redshift z .

We point out that the red sequence that is identified by our two-step procedure is more robust towards contamination by interlopers than a red sequence that is obtained, e.g., by keeping the slope fixed to a value derived from local samples of ETGs (e.g., Bell et al. 2004a). Using a non-optimally chosen slope introduces undesirable effects since this basically determines the fraction of faint galaxies in the resulting red sequence selected sample. Estimates for the slope of the $z = 0$ red-sequence in local galaxy clusters range from -0.12 to -0.02 , depending on the aperture adopted for the measurements (Scodreggio 2001). Assuming a too steep slope for the data under study would lead to the inclusion of a large fraction of faint blue interlopers.

The final red sequence defines our *photometrically-selected sample* of high- z progenitors of $z = 0$ ETGs. This sample includes all galaxies with $U - V$ color redder than the value corresponding to “minus 3σ ” from the final red sequence at the appropriate redshift, i.e., $U - V = 1.53 - 0.37z - 0.035(M_V + 20)$. The sample contains 3844 galaxies with $I_{AB} \leq 24$ and photometric redshift in the range $0.2 < z \leq 1.0$ ⁴.

The right panel of Figure 2 highlights in color the galaxies which belong to this photometrically-selected sample, and specifically in red the galaxies that have a ZEBRA elliptical-galaxy fit, and in blue those with ZEBRA late-type spectral fits. Below (Section 4.2) we argue that it is sensible to apply the Kormendy-test described above also to the so-derived photometrically-selected sample; we will thus define as final photometrically-selected sample those galaxies in

⁴Bell et al. (2004a) found ~ 4700 red-sequence selected galaxies in the redshift range $0.2 < z < 1.1$ down to $R_{VEGA} = 24$ in the COMBO17 survey, in an area similar to the COSMOS area presented here. If we consider the same redshift range, and relax our constrain on the accuracy of the photometric redshift we find $\sim 12\%$ more photometrically-selected COSMOS ETGs than COMBO17. This is consistent with our being and $I_{AB} = 24$ selected sample and their being a $R_{VEGA} = 24$ selected sample. We also stress that ours and Bell et al.’s samples are not directly comparable, since Bell et al. fixed the red-sequence slope to the value of -0.08 found in local galaxy clusters, while we consistently compute the red-sequence slope, from the observed color–magnitude diagram.

the sample constructed so far that also pass the "Kormendy-test".

4. Properties of the morphologically- and photometrically-selected early-type galaxies

4.1. Colors of morphologically-selected galaxies

In Figure 5 we show, separately for the considered four redshift bins, the $(U - V)$ - M_V color-magnitude diagram for the Kormendy-test-consistent, morphologically-selected sample of early-type galaxies discussed in Section 3.1. In particular, black filled circles show the ZEST Type 1 early-type galaxies, and cyan circles represent the bulge-dominated Type 2.0 disk galaxies. The red line in each panel reproduces the final red-sequence –calculated at the center of the redshift bin– derived in Section 3.2.2. At any redshift, the majority of morphologically-selected early-type galaxies is characterized by red colors (consistent with the final red sequence defined above); however, a fraction of order 40% of these systems has significantly bluer colors than the red sequence (see Tables 1 and 2). These galaxies would be missed in a pure color-based selection. This fraction is similar to that of morphologically-selected galaxies at $z = 0$ that do not belong to the red-sequence, see Table 1 in Renzini (2006). The morphologically-selected sample of ETG progenitors covers the entire observed range of rest-frame $(U - V)$ colors, although very few of them have $U - V < 0.5$. This is not a consequence of the Kormendy-relation selection that has been applied to the sample: this is demonstrated by the black dots in each panel, which show the galaxies with morphological Type 1 + 2.0 that are excluded from the final morphological sample on the basis of the Kormendy-test. These "Kormendy-test-rejected" galaxies are typically faint systems (of order $M_V > -19.5$); there is however no obvious dependence of this galaxy population on the $U - V$ color.

As evident from Figure 5, the color distributions of ZEST Type 1 and Type 2.0 galaxies are rather similar (apart from a small blue "excess" at low redshifts of bulge-dominated disks at bright magnitudes). This is further illustrated in Figure 6, where the rest-frame $U - V$ color distributions are shown for both types as solid and dashed histograms, respectively. In each redshift bin, the Type 1 and Type 2.0 samples are split in two components, one brighter (left panels) and the other fainter (right panels) than the value of M_B^* at the center of the given redshift bin; the M_B^* values are derived from the Schechter fits discussed in Section 5, and are given in the top-right corner of each diagram.

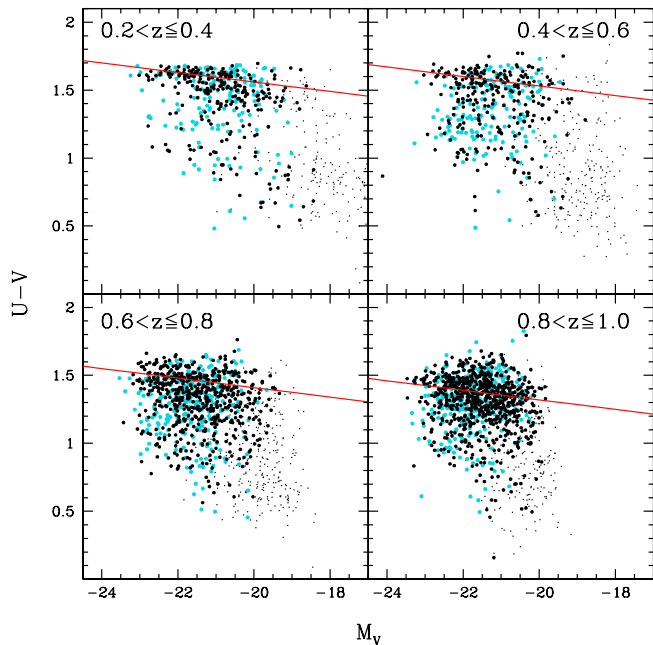


Fig. 5.— Rest-frame color–magnitude diagram $U - V$ versus M_V for the morphologically-selected sample of ETGs. Black and cyan filled circles are used for galaxies kept in the sample, after passing the Kormendy-relation test described in Section 3.1.1. Black filled circles are used for the ZEST Type 1 (early-type morphology) galaxies, while cyan filled circles are used for the ZEST Type 2.0 (bulge-dominated disk) galaxies. Black dots show the galaxies that were excluded from the morphologically-selected sample on the basis of the Kormendy test. The red line in each panel reproduces the final red-sequence derived in Section 3.2.2 calculated at the center of the redshift bin.

4.2. Morphology & structure of photometrically-selected galaxies

In the left panel of Figure 7 we show the fractions of photometrically-selected early-type galaxies (derived in Section 3.2), that belong to different ZEST morphological classes. To make the comparison among different redshift bins meaningful, we limit the analysis to $M_B = -19$ at redshift $z = 0.9$, and we evolve this magnitude limit as a function of redshift according to the evolution of a single-burst stellar population formed at $z_f = 2$; according to the relation $\Delta M_B = -1.36z$ (c.f. Section 3.1.1).

In Figure 7, Type 1 early-type galaxies and Type 2.0 bulge-dominated galaxies are considered as a single class (labelled with “1 + 2.0”). The results for the four redshift bins are represented with different colors (as described in the Figure). Galaxies with early-type morphologies, i.e., the combined sample of Type 1+2.0 galaxies, contribute from $\sim 45\%$ at

$z = 0.9$ to $\sim 60\%$ at $z = 0.3$ to the sample of photometrically-selected ETGs. This compares to the fraction of $\sim 58\%$ at $z = 0$ (Renzini 2006). The majority of the galaxies that are not classified as early-type Type 1 or Type 2.0 galaxies have the morphology of disk-dominated, small-bulge galaxies ($\sim 30\%$ and 20% of ZEST Type 2.1 and 2.2, respectively); the remaining few percents are almost equally split between bulgeless disks (Type 2.3) and irregular galaxies (Type 3).

Bell et al. (2004b) presented the morphological distribution of a sample of COMBO17 red-sequence selected galaxies with redshifts between $0.65 \leq z < 0.75$. They find that, down to $M_V = -20.3$, 85% of the combined rest-frame V -band luminosity density comes from visually classified E/S0/Sa galaxies. A slightly smaller fraction (75%) was found by McIntosh et al. (2005) using an automatic morphological classification for early-type galaxies based on the Sersic index n . When limiting the analysis of the COSMOS data to the same bright cut in M_V magnitude and considering the same redshift range, we find that a similar fraction of $\sim 75\%$ of the rest-frame V -band luminosity density comes from Type 1 + 2.0 ETGs.

4.2.1. Kormendy-test selection of the photometric sample

In principle, mergers of old stellar sub-units “caught in the act” could have irregular morphologies and not satisfy the Kormendy-test described above. We nonetheless investigate which fraction of the photometrically-selected sample is excluded on the basis of this test, and which are the properties of the rejected objects.

In Figure 8 we show the Kormendy diagram for the photometrically-selected sample of ETGs, split in the four redshift bins; symbols and lines are as in Figure 1. In this Figure we also identify all galaxies that have an irregular (ZEST Type 3) morphological classification by large black circles. Indeed, not all of the red-sequence selected galaxies are consistent with passively-evolving into the Kormendy relation at redshift $z = 0$. Interestingly, however, the vast majority of galaxies that are excluded on the basis of the Kormendy criterion have a regular (ZEST Type 1 or 2) morphology. This is illustrated in the right panel of Figure 7, where we show the morphological mixture of photometrically-selected galaxies which do not pass the Kormendy-test. Only up to $\sim 2\%$ of these Kormendy-test-rejected galaxies have the Type 3 irregular morphology. This is consistent with the rather short (< 1 Gyr) timescales during which major dissipationless mergers appear as one irregular systems. At all redshifts, the vast majority ($> 70\%$) of Kormendy-test-rejected objects in the photometrically-selected sample are disk-dominated galaxies. Therefore, when studying the redshift evolution of the LFs of plausible ETG progenitors, it seems appropriate to apply

the Kormendy-test-rejection criterion also to the photometrically-selected sample, as already done for the morphologically-selected sample. We thus indicate with *final photometrically-selected* sample the 2877 galaxies, selected according to the red-sequence criterion described in Section 3.2, that furthermore pass the Kormendy-test. We will nevertheless also show, in our analysis of the LFs, the results obtained when no Kormendy-selection is performed on the galaxy samples under study.

4.3. The combined sample of progenitors of $z=0$ ellipticals

There is, obviously, overlap between the morphologically- and photometrically-selected samples, as shown in Figures 5 and Figure 7. We therefore also present, in the following, the analysis for the *combined sample* of all plausible candidate ETG progenitors at each redshifts, i.e., *the union of the above-defined morphologically- and photometrically-selected samples*. This combined sample contains a total of 3980 galaxies; specifically, 1623 of the 2730 galaxies in the final morphologically-classified sample are also members of the final photometrically-classified sample (see Tables 1 and 2).

4.4. Summary of the selected final samples

For easy reference we summarize in Tables 1 and 2, as a function of redshift, the number of galaxies contained in the morphological, photometric and combined final samples, and the relative fraction of galaxies in common between the morphological and photometric samples.

5. The redshift evolution of the LF of early-type galaxies in COSMOS

We derive the B -band LFs using the $1/V_{\max}$ estimator (Schmidt 1968; Felten 1976): The number of galaxies per unit comoving volume in the range of absolute magnitudes dM , at redshift z , and belonging to the sample S can be written as:

$$\int \Phi_S(M, z) dM = \sum_S \frac{1}{V_{\max,i}}, \quad (3)$$

where the sum is over all galaxies in the sample S within the specific range of redshift and absolute magnitude. $V_{\max,i}$ is the maximum comoving volume within which a galaxy

Table 1. Final samples of ETGs

$z(\text{Range})$	MORPHO	PHOTO	COMBINED
$0.2 < z \leq 0.4$	414	422	574
$0.4 < z \leq 0.6$	414	407	594
$0.6 < z \leq 0.8$	862	824	1214
$0.8 < z \leq 1.0$	1040	1224	1598
TOTAL	2730	2877	3980

Note. — Number of galaxies in the final morphologically-selected (MORPHO), and photometrically-selected (PHOTO) samples, splitted in the four redshift bins. The number of galaxies per redshift bin in the combined sample are also listed.

Table 2. Overlap in the galaxy final samples

$z(\text{Range})$	MORPHO in PHOTO	PHOTO in MORPHO
$0.2 < z \leq 0.4$	63%	61%
$0.4 < z \leq 0.6$	54%	55%
$0.6 < z \leq 0.8$	55%	57%
$0.8 < z \leq 1.0$	65%	54%

Note. — Listed are, split in the four redshift bins, the fraction of morphologically-selected galaxies present in the photometrically-selected sample, and the fraction of photometrically-selected galaxies present in the morphologically-selected sample.

i could still be detected, given the apparent magnitude limits of the survey, i.e., in our study, $16 \leq I_{AB} \leq 24$; the volume is appropriately corrected so as to account for the (small) fraction of objects that were excluded from the initial ACS-selected sample due to the lack of photometric redshifts. More specifically, $V_{\max,i}$ is the comoving volume between z_1 and z_2 , computed, for each galaxy i , taking into account the k -correction as a function of redshift. The z_1 and z_2 values are, respectively, the maximum between z_L and z_{16} , and the minimum between z_U and z_{24} ; the limiting values z_U and z_L are the upper and lower redshift of the considered redshift bin, and z_{24} and z_{16} are the redshifts at which the galaxy i would have an I_{AB} apparent magnitude of 24 and 16, respectively, for a given rest-frame B -band absolute magnitude and color.

The $1/V_{\max}$ estimator approach does not correct for sources that are missed from the input catalog due to selection effects. In particular, a catalogue that is defined according to a magnitude cut in a given passband suffers from color-dependent selection effects (e.g. Lilly et al. 1995). In our $I_{AB} \leq 24$ sample, blue objects are detected down to fainter absolute B magnitudes for redshifts higher than $z \sim 0.8$, i.e., the redshift at which the observer-frame I -band coincides with the rest-frame B -band; below $z \sim 0.8$, it is the red objects that are instead detected to fainter absolute B magnitudes. Correcting for this bias is not straightforward, as it requires an assumption on the color distribution of the galaxy population that is missed from the sample. To avoid this potential source of error, we therefore limit the computation of the LF in each redshift bin to the luminosity range for which we are complete, regardless of galaxy colors.

In Figure 9 we show, split in four redshift bins, the LFs computed for the different samples of ETGs described in the previous Sections. Specifically, the green, red and black curves represent respectively the *final morphologically-selected* sample, the *final photometrically-selected* sample (i.e., both after the Kormendy-test cut), and the *combined* sample of all plausible progenitors of $z = 0$ ETGs, which are selected either due to their morphology or to their colors. The error bars in each luminosity bin take into account Poissonian errors only. In Appendix A we discuss all other sources of errors, and their impact on the LFs. In particular, we show in the Appendix that our main conclusions are largely unaffected by uncertainties in the photometric redshift errors.

In the four panels of Figure 9, we highlight the effects of cutting the sample according to the Kormendy-test. In particular we show, with black empty symbols and thin lines, the LFs resulting from the morphologically- (solid) and photometrically-selected (dashed) samples when the kormendy-relation constraint is not applied. At all redshifts, the inclusion of galaxies that are rejected on the basis of the Kormendy-test would lead to a substantial increase in the number of ETGs at the faint end ($M_B > -20$) of the LFs.

Figure 9 shows that at all redshifts, the shape of the LFs of the final morphologically- and photometrically-selected samples of ETGs are very similar. However, at magnitudes brighter than $M_B \sim -21$, morphologically-selected, i.e., dynamically-relaxed, early-type galaxies tend to be more numerous than photometrically-selected, i.e., old-stellar-population galaxies, by up to a factor of 2. In contrast, photometrically-selected ETGs are more numerous relatively to the morphologically-selected by about the same factor at fainter magnitudes. From the lowest up to the highest redshift bin, respectively about $90 \pm 10\%$ to $75 \pm 10\%$ of the final sample of photometrically-selected ETGs brighter than $M_B = -21 - 1.4z$ also belong to the morphologically-selected sample.

These results suggest that, at all redshifts under study, the majority of the most massive ETGs are already dynamically-relaxed systems with the appearance of $z = 0$ elliptical galaxies and their stellar populations are passively evolving, which is consistent with other features of the LFs that we discuss in Section 6.

We fit a Schechter function (Schechter 1976) to the COSMOS LFs, to derive for them an analytical description. The Schechter function best-fit parameters, i.e., the characteristic magnitude M_B^* , the volume density at M_B^* , Φ_* , and the slope of the faint-end, α , are derived adopting a χ^2 procedure. The best fit parameters for the Schechter fits are shown in Table 3. The relatively high normalization factor in the lowest redshift bin is due to the well known overdensity in the central region of the COSMOS field (which is also a reason for using the SDSS to determine the cosmic evolution of the LFs in the $z = 1$ to $z = 0$ window). In the fits, the faint-end slope α is allowed to vary, and α values in the range ≈ 0.1 - 0.6 are derived, with *formal* 1σ errors of about $\sigma_\alpha \approx 0.1$; these values are different from the $\alpha \sim -0.6$ value adopted by, e.g., Bell et al. (2004a). However, these values of α are derived on the Kormendy-consistent samples, and are therefore not directly comparable with those used by other authors. The faint end slope in the highest redshift bin is however not well defined, given the magnitude cut of our sample; furthermore, despite the variations in α values, all the measurements are consistent within 3σ with a constant faint end slope. Thus, all in all, the analytical fits quantitatively demonstrate the similarity, discussed above, of the LFs as a function of redshift.

5.1. The $z = 0$ comparison sample

The volume of Universe covered by the Cycle 12 COSMOS data in the redshift range $0 < z \leq 0.1$ is only $\sim 5.5 \times 10^3 \text{ Mpc}^3$, and includes less than 50 galaxies; therefore, cosmic variance and small number statistics make this bin inadequate for comparisons with the

Table 3. Schechter Function best-fit parameters

z (Range)	Φ^* ($\text{Mpc}^{-3} \text{Mag}^{-1}$)	M_B^* (mag)	α
(1)	(2)	(3)	(4)
Final morphologically-selected sample			
0.2–0.4	0.0025 ± 0.0001	-20.34 ± 0.10	0.28 ± 0.11
0.4–0.6	0.0010 ± 0.0001	-20.38 ± 0.12	0.64 ± 0.12
0.6–0.8	0.0014 ± 0.0001	-20.70 ± 0.07	0.60 ± 0.09
0.8–1.0	0.0013 ± 0.0001	-20.76 ± 0.12	0.42 ± 0.13
Final photometrically-selected sample			
0.2–0.4	0.0025 ± 0.0001	-20.22 ± 0.12	0.12 ± 0.13
0.4–0.6	0.0010 ± 0.0001	-20.14 ± 0.10	0.43 ± 0.13
0.6–0.8	0.0013 ± 0.0001	-20.55 ± 0.08	0.38 ± 0.09
0.8–1.0	0.0017 ± 0.0001	-20.62 ± 0.07	0.21 ± 0.10
Combined Sample			
0.2–0.4	0.0034 ± 0.0001	-20.28 ± 0.10	0.12 ± 0.11
0.4–0.6	0.0015 ± 0.0001	-20.37 ± 0.08	0.40 ± 0.09
0.6–0.8	0.0019 ± 0.0001	-20.63 ± 0.06	0.47 ± 0.07
0.8–1.0	0.0021 ± 0.0001	-20.73 ± 0.07	0.23 ± 0.08

Note. — The columns are: (1) Redshift range; (2) Schechter function normalization Φ^* , and error; (3) M_B^* , and error; (4) Slope of the faint end, α , and error. The fits are performed on the *final* morphologically- and photometrically-selected samples, i.e., after the Kormendy-test cut, and on the combined sample derived from these final sub-samples.

higher redshift bins to trace galaxy evolution down to $z = 0$. Furthermore, the $0.2 < z \leq 0.4$ redshift bin is affected by a relatively strong overdensity (Scoville et al. 2007b).

Therefore, following the approach described in Paper I, in order to study the evolution of the LFs from $z \sim 1$ to $z = 0$, we compare the COSMOS LFs with a complete sample of galaxies extracted from the Sloan Digital Sky Survey (York et al. 2000), appropriately redshifted to $z = 0.7$ so as to provide a direct calibration point for the $0.6 < z \leq 0.8$ COSMOS data. The generation of the redshifted SDSS images is described in Kampczyk et al. (2007), and also summarized in Paper I and in Appendix B. The SDSS redshifted images were analyzed following the identical procedure that was adopted for the COSMOS galaxies: *(i)* The SDSS galaxies were morphologically classified with ZEST; *(ii)* The photometrically-selected sample of SDSS early-type galaxies was determined according to the two-step procedure described in Section 3.2; *(iii)* The Kormendy-cut was applied to both the photometrical and morphological samples of ETG progenitors; and *(iv)* Finally, the LFs for the morphologically-selected, photometrically-selected and combined samples of redshifted SDSS ETGs were calculated, using the approach described in Section 5. We stress that by applying exactly the same procedure to the COSMOS and to the SDSS samples, the same systematics apply to both the high- z and the local comparison sample. Thus, the direct comparison of the two allows us to identify, without biases, any evolutionary effect of the galaxy samples under study from $z = 0.7$ to $z = 0$.

6. Discussion

In Figure 10 we compare the $0.6 < z \leq 0.8$ COSMOS LFs (solid lines) with the redshifted SDSS LFs (thick dashed lines) for the morphologically-selected, photometrically-selected and combined samples of ETGs. The thin dashed curves represent the SDSS LFs after brightening by ~ 0.95 magnitude, i.e., the luminosity evolution from $z = 0.7$ to $z = 0$ consistent with the observed evolution of the red-sequence discussed in Section 3.2.2.

At luminosities higher than $\sim 2.5 - 3 L^*$ (i.e., ~ 1 mag brighter than $M_B^* \approx -20.7$, see Table 3), the $z \sim 0.7$ COSMOS LF of the photometrically-selected sample of ETGs well matches the bright end of the corresponding SDSS LF, after applying the brightening of 0.95 magnitudes. The number density of the brightest –and thus most massive– photometrically-selected ETGs does not evolve from redshift $z = 0.7$ to redshift $z = 0$. At fainter magnitudes, however, the number density of photometrically-selected early-type galaxies shows an increase of a factor up to three from $z \sim 0.7$ to $z = 0$. We stress that the sample of bright photometrically-selected ETGs is not contaminated by dusty disks. Indeed, we found that the fraction of Type 1+2.0 in the photometrically-selected sample of ETGs

at redshift $z = 0.7$ is $\sim 90\%$ for galaxies brighter than $M_B = -21.7$.

Broadly speaking, a similar result is obtained also for the morphologically-selected and combined samples of early-type galaxies. However, adopting a similar evolution as above, the number density of the brightest, $M_B < -21.7$ morphologically-selected Type 1 + 2.0 ETGs at $z \sim 0.7$ in the COSMOS field would slightly exceed the number density of the brightened SDSS sample. This suggests a faster luminosity evolution for the morphologically-selected sample of ETGs, which is consistent with the latter containing a fraction of galaxies with colors bluer than those predicted for a passively evolving stellar population (see Section 4.1). These blue colors might arise from a substantial fraction of mass in intermediate-age stars. However, a recent second bursts of star formation, producing only a few percent of the stellar mass, would also make significantly bluer the colors of the stellar population and increase the B -band luminosity of the galaxies.

For example, adding a 1 to 5% stellar mass in a second burst of star formation to an underlying old, single-burst population with formation redshift $z_f = 2$ is sufficient to explain the $U - V$ colors of even the bluest morphologically-selected ETGs at all redshifts under study. This suggests that the bulk of the stellar mass in *all* morphologically-selected high- z ETGs is already formed by $z \sim 1$. This is consistent with the other studies that we have already mentioned, which find that $z \sim 0.3 - 0.75$ galaxies with $M \geq 10^{11} M_\odot$ have an integrated specific star formation rate less than the global value. These studies conclude that the bulk of star formation in massive galaxies occurs at early cosmic epochs and is largely complete by $z \sim 1.5$, and that further mass assembly in these galaxies takes place with low specific star formation rates (e.g., Dickinson et al. 2003; Papovich et al. 2006).

Furthermore, similar to the case of the photometrically-selected progenitors of ETGs, also the morphologically-selected sample and the combined sample of early-type galaxy progenitors show a remarkable lack of evolution of the very bright-end of their LF. Fainter early-type galaxies are instead again about a factor $\sim 2 - 3$ less numerous than at $z = 0$.

More quantitatively, we compute the total density of ETGs brighter than $2.5 L^*$ in both the combined sample of COSMOS and SDSS ETGs. We indicate these two densities with ρ_{COSMOS} and ρ_{SDSS} , respectively. The adopted value of L^* is the one derived from the Schechter fit to the $z = 0.7$ LF of the combined sample (see Table 3). In order to compute ρ_{SDSS} , we integrate the SDSS local LF brightened by 0.95 magnitudes. Consistent with the qualitative analysis presented above, we find that

$$\rho_{\text{COSMOS}}/\rho_{\text{SDSS}} = \frac{(2.32 \pm 0.17) \times 10^{-4}}{(2.38 \pm 0.20) \times 10^{-4}} = 0.97 \pm 0.11. \quad (4)$$

The density of $L > 2.5L^*$ ETGs remains constant, within the Poissonian errors, since $z = 0.7$ to today. This conclusion might in principle depend on the assumed amount of luminosity evolution (i.e., the SFH of the ETG population), on the cosmic variance, and on the effect of the photometric redshift uncertainties on the LFs. As we discuss in Appendix A and Section 5, Poissonian errors at such bright magnitudes are, however, larger than the uncertainties on the LF induced by the errors on the photometric redshifts. Errors due to the photo- z can thus be neglected.

The effect of cosmic variance on ρ_{COSMOS} can be quantified using the prescription of Somerville et al. (2004). We estimate that, for the given density and COSMOS volume, this uncertainty contributes at most $\sim 25\%$ to the error on ρ_{COSMOS} . We obtain a similar result by calculating the variance of the total number of $M_B < -21.7$, i.e. $> 2.5L^*$, galaxies in the 24 mock galaxy catalogs generated by Kitzbichler et al. (2007) for the COSMOS survey using the Millennium Run numerical simulations. The SDSS density, ρ_{SDSS} , is not affected by cosmic variance, since the 1800 SDSS galaxies were chosen randomly in a local volume larger than $2 \times 10^5 \text{ Mpc}^3$, and the derived SDSS LF closely matches the Blanton et al. (2003) LF derived from the entire SDSS galaxy catalog (see further discussion in Kampczyk et al. 2007).

What causes the largest uncertainty in ρ_{SDSS} is the assumed luminosity evolution for the ETG stellar population. In the previous analysis we have used the evolution of a single stellar population formed at redshift $z_f = 2$, justified by the fact that this SFH is consistent with the observed evolution of the red-sequence zero point (see Section 3.2.2). However, we can estimate the changes induced on ρ_{SDSS} due to a reasonable range of SFHs, and use them as more realistic estimates of the errors on ρ_{SDSS} . Although the range of observed $d(M/L)/dz$ reported in the literature is broad (see, e.g., Table 2 in Treu et al. 2005, and references therein), a recent study by van Dokkum & van der Marel (2006) shows that stars in massive ETGs ($M > 10^{11} M_\odot$), both in clusters and in the field, have a mean luminosity-weighted formation redshift of $z_f = 2.01^{+0.22}_{-0.17}$. For such massive galaxies, Thomas et al. (2005) show that the star-formation time scale is less than 1 Gyr, which therefore makes our z_f a reasonable approximation for the measured value. This formation timescale, together with the error on z_f presented by van Dokkum & van der Marel (2006), can be used to derive the uncertainty on ρ_{SDSS} due to varying the luminosity evolution of the ETGs. We find that an uncertainty in formation redshift of $\Delta z_f = 0.4$ corresponds, roughly, to a $\Delta(M_B) = 0.1$ at a redshift $z = 0.7$. It follows that the total density of $M_B = -21.7 \pm 0.1$ ETGs in the combined sample is $\rho_{SDSS} = (2.38 \pm 0.42) \times 10^{-4} \text{ Mpc}^{-3}$. It is clear, then, that the largest source of uncertainty on ρ_{SDSS} is indeed due to the assumed SFH.

Considering together the effects of cosmic variance and varying the SFHs, the ratio

between the observed and predicted density of massive ETGs at redshift $z = 0.7$ is therefore $\rho_{\text{COSMOS}}/\rho_{\text{SDSS}} = 0.97 \pm 0.32$. This shows that bright ($L > 2.5 L_*$) ETGs are already in place at $z = 0.7$, and that the maximum evolution in the number of bright ETGs allowed from $z = 0.7$ to $z = 0$ is at most of $\sim 30\%$.

In contrast, there is indeed a dearth of lower-luminosity ETGs, at $z \sim 0.7$ compared with the local universe. This deficiency of intermediate-to-faint ETGs is not an effect of incompleteness, since (i) both in the morphologically- and photometrically-selected samples, the deficit of early-type galaxies is visible at magnitudes $M_B \sim -21$, i.e., well above our magnitude limit ($M_B \sim -18.5$ at $z = 0.7$); (ii) the central wavelength of F814W filter matches the rest-frame B -band at $z = 0.8$; this implies that, down to the faintest magnitude bin considered, there are no color-dependent selection effects in the redshift range $0.6 < z < 0.8$; (iii) the ZEST classification recovers the morphological class for $\sim 80\%$ of the galaxies down to $I_{AB} = 23$ (Paper I); furthermore, possible systematics in the morphological classification are identical for the COSMOS and for the local SDSS sample used to normalize our results.

Arguments for an apparent anti-hierarchical mass assembly of ETGs were recently presented based on the redshift evolution of the mass function (Bundy et al. 2005) and of the luminosity function (Cimatti, Daddi & Renzini 2006, Brown et al. 2007, Wake et al. 2006). Furthermore, enough star-formation is observed in massive galaxies at higher redshifts to account for all stars that we observe already assembled in massive galaxies by $z \sim 1$ (Daddi et al. 2005). Our morphological selection of ETGs adds to this picture the key information that not only the full mass assembly of the most massive ETGs was completed at an earlier cosmic time compared to the less massive galaxies, but also that the majority of these systems achieved dynamical relaxation by $z \sim 1$. A relatively large fraction of the less massive early-type galaxies has either not yet achieved relaxation at the redshift (epoch) at which they are observed, or not completed its star-formation.

7. Concluding remarks

We highlight our three main results: (1.) The shapes of the LFs of morphological, photometrical and combined samples of ETG progenitors at all redshifts are remarkably similar; (2.) The vast majority of photometrically-selected massive ETGs is already dynamically-relaxed –and has thus the morphology of an early-type galaxy– at redshifts $z \sim 1$; and (3.) There is a deficiency of approximately $< 2L^*$ ETGs as opposed to remarkable constancy of the bright end ($L > 2.5L^*$) of the LFs of morphologically- and photometrically-defined ETGs.

These findings support a scenario in which the brightest, most massive early type galaxies are already fully assembled ~ 8 Gyrs ago, while fainter, less massive early-type galaxies keep forming their stars and assembling their mass from $z = 0.7$ to the present. This trend in the observed evolution of the LFs of early-type galaxies, together with the observed constancy with redshift of the LFs' shapes, argues against a significant contribution of dry mergers in the build up of the $z = 0$ massive ETG population. Furthermore, we suggest that the $z = 0$ lower luminosity early-type galaxies are the end product of the conversion of blue irregular and disk galaxies into 'red', early-type galaxies. This explanation is also supported by the observed increase of about a factor of three in the number density of irregular galaxies from the local Universe to $z = 0.7$ (Paper I).

REFERENCES

- Abraham, R. G., van den Bergh, S., & Nair, P. 2003, ApJ, 588, 218
- Bell, E. F., et al. 2004a, ApJ, 608, 752B
- Bell, E. F., et al. 2004b, ApJ, 600, L11
- Bell, E. F., et al. 2006a, ApJ, 640, 241
- Bell, E. F., Phleps, S., Somerville, R. S., Wolf, C., Borch, A., & Meisenheimer, K. 2006b, ApJ, 652, 270
- Bender, R., Burstein, D., & Faber, S. M. 1993, ApJ, 411, 153
- Bernardi, M., et al. 2003a, AJ, 125, 1882
- Bernardi, M., et al. 2003b, AJ, 125, 1849
- Bernardi, M., et al. 2003c, AJ, 125, 1866
- Bertin, E., & Arnouts, S. 1996, A&AS, 117, 393
- Blanton, M. R., et al. 2003, ApJ, 594, 186
- Bower, R. G., Lucey, J. R., & Ellis, R. S. 1992, MNRAS, 254, 601
- Brown, M. J. I., et al., 2007, ApJ, 654, 858
- Bruzual, G. & Charlot, S., 2003, MNRAS, 344, 1000
- Bundy, K., Ellis, R. S., & Conselice, C. J. 2005, ApJ, 625, 621

- Carollo, C. M., Danziger, I. J., & Buson, L. 1993, MNRAS, 265, 553
- Carollo, C. M., & Danziger, I. J. 1994a, MNRAS, 270, 743
- Carollo, C. M., & Danziger, I. J. 1994b, MNRAS, 270, 523
- Capak, P. et al. 2007, ApJS, submitted
- Cimatti, A., Daddi, E., & Renzini, A. 2006, A&A, in press (astro-ph/0605353)
- Coleman, G. D., Wu, C.-C., & Weedman, D. W. 1980, ApJS, 43, 393
- Daddi, E., et al. 2005, ApJ, 631, L13
- Dickinson, M., Papovich, C., Ferguson, H. C., Budavri, T., 2003, ApJ, 587, 25
- Djorgovski, S., & Davis, M. 1987, ApJ, 313, 59
- Dressler, A., Faber, S. M., Burstein, D., Davies, R. L., Lynden-Bell, D., Terlevich, R. J., & Wegner, G. 1987, ApJ, 313, L37
- Faber S.M., Willmer C. N. A., Wolf C., Koo D. C., Weiner B. J., et al. 2005, ApJ, submitted (astro-ph/0506044)
- Feldmann, R. et al., 2006 MNRAS, 372, 565
- Felten, J. E. 1976, ApJ, 207, 700
- Ferreras, I., Lisker, T., Carollo, C. M., Lilly, S. J., & Mobasher, B. 2005, ApJ, 635, 243
- Hogg D., 2006. In *The Fabulous Destiny of Galaxies: Bridging Past and Present*, ed. V Le Brun, A Mazure, S Arnouts, & D Burgarella. Paris:Edition Frontieres, In press (astro-ph/0512029)
- Jørgensen, I., Franx, M. & Kjaergaard, P., 1995, MNRAS, 273, 1097
- Kampczyk, P. et al. 2007, ApJS, accepted, (astro-ph/0611187)
- Kitzbichler et al. 2007, MNRAS, submitted
- Kinney, A. L., Calzetti, D., Bohlin, R. C., McQuade, K., Storchi-Bergmann, T., & Schmitt, H. R. 1996, ApJ, 467, 38
- Koekemoer, A. et al. 2007, ApJS, submitted
- Kodama, T., Arimoto, N., Barger, A. J., & Arag'on-Salamanca, A. 1998, A&A, 334, 99

- Kormendy, J. 1977, ApJ, 218, 333
- Leauthaud, A. et al. 2007, ApJS, submitted
- Lilly, S. J., Tresse, L., Hammer, F., Crampton, D., & Le Fevre, O. 1995, ApJ, 455, 108
- Lilly, S. et al. 2007, ApJS, submitted
- Lin, L., Koo, D. C., Willmer, C. N. A., Patton, D. R., Conselice C. J., et al. 2004. ApJ, 617, L9
- Lotz, J. M., Primack, J. & Madau, P. 2004, AJ, 128, 163
- Masjedi M, Hogg DW, Cool RJ, Eisenstein DJ, Blanton MR, et al. 2006. ApJ, 644, 54
- McIntosh, D. H., et al. 2005, ApJ, 632, 191
- Oke, J. B. 1974, ApJS, 27, 21
- Papovich, C., et al. 2006, ApJ, 640, 92
- Petrosian, V. 1976, ApJ, 209, L1
- Renzini, A. 2006, ARA&A, 44
- Rix, H.-W., et al. 2004, ApJS, 152, 163
- Sargent M., et al. 2007, ApJS, accepted (astro-ph/0609042)
- Scarlata, C. et al. 2007, ApJS, accepted, (astro-ph/0611644)
- Schechter, P. 1976, ApJ, 203, 297
- Schmidt, M. 1968, ApJ, 151, 393
- Scodeggio, M. M. 2001, AJ, 121, 2413
- Scoville, N. et al. 2007a, ApJS, accepted
- Scoville, N. et al. 2007b, ApJS, accepted
- Somerville, R. S., Lee, K., Ferguson, H. C., Gardner, J. P., Moustakas, L. A., & Giavalisco, M. 2004, ApJ, 600, L171
- Springel, V., Frenk, C.S. & White, S.D.M. 2006, Nature, 440, 1137
- Strauss, M. A., et al. 2002, AJ, 124, 1810

- Taniguchi, Y. et al. 2006, ApJS, this volume
- Thomas, D., Maraston, C., Bender, R., & Mendes de Oliveira, C. 2005, ApJ, 621, 673
- Treu, T., et al. 2005, ApJ, 633, 174
- van Dokkum, P. G., & Stanford, S. A. 2003, ApJ, 585, 78
- van Dokkum, P. G., 2005, AJ, 130, 2647
- van Dokkum P. G, & van der Marel, R. P., 2006, ApJ, in press
- Wake, D. A., et al. 2006, MNRAS, 372, 537
- York, D. G., et al. 2000, AJ, 120, 1579

A. Impact of photo- z uncertainties on LFs

Feldmann et al. (2006) estimated the quality of the photometric redshifts by comparison with spectroscopic redshifts for a sample of 866 galaxies observed within the z -COSMOS survey (Lilly et al. 2007). The comparison shows that the ZEBRA photometric redshifts have an accuracy of $\sigma_z \propto 0.027(1+z)$ for galaxies brighter than $I_{AB} = 22.5$, and with redshift $z \leq 1.2$. In order to estimate the accuracy at magnitudes fainter than $I_{AB} = 22.5$, we simulated a faint version of the spectroscopic redshift catalog by dimming the $I_{AB} \leq 22.5$ galaxies with available spectroscopic redshift down to our magnitude limit of $I_{AB} = 24$. We then recomputed the ZEBRA photometric redshifts for these artificially-faint sources. The accuracy of the ZEBRA photo- z 's down to $I_{AB} = 24$ is $\sigma/(1+z) \sim 0.06$.

To estimate the effect of the photometric uncertainties on the calculation of the LFs, we create one hundred versions of the COSMOS catalog, by convolving the measured photometric redshift with the photometric redshift error appropriate for the magnitude of each object. We consider two bins of magnitude: for all galaxies with $I_{AB} \leq 22.5$ we used $\sigma_z = 0.03(1+z)$, while we use $\sigma_z = 0.06(1+z)$ for all galaxies with $22.5 < I_{AB} \leq 24.0$. Although the photometric redshift errors should be applied to an “error-free” catalog, our test provides a conservative estimates of how important the effects of the photometric redshift errors are on the observed LFs.

Using the simulated COSMOS catalogs we extracted 100 versions of the morphologically- and photometrically selected samples of ETGs, following the procedures described in Sections 3.1 and 3.2. We computed the LFs for these 100 re-simulated samples using the procedure described in Section 5.

In Figure 11 we present the results of this test in the redshift range $0.6 < z \leq 0.8$. This is the redshift range we use to derive the main conclusions of our paper. In Figure 11 solid circles with errorbars represents the LF computed using the “true” photometric redshifts, and the open red circles represent the median of the 100 realizations. The shaded grey area associated with the simulated volume densities represent the 16th and 84th percentiles of the simulated distributions within each magnitude bin. Figure 11 shows that the dominant effect of the redshift uncertainty is at the faint end of the LF, where the number of galaxies is sistematically higher in the error-convolved LFs. This effect is stronger in the color selected samples than in the morphologically selected one.

At the bright end, the only significant effect is for very bright magnitudes ($M_B < -23$, i.e., $L > 10L_*$), where we would overestimate the number of galaxies. Indeed, in the simulations we find 1 – 2 galaxies with these magnitudes in 8 out of the 100 mock realizations. These resultss are consistent with those of Brown et al. (2007) who performed similar simulations and find that the effect of photometric redshfit errors on the LF is only significant for $M_B - 5 \log(h) < -22.5$. We note however, that no such galaxies are observed in the original COSMOS catalog. These tests show that, for the area covered by the present analysis, Poissonian errors dominate the contribution in the error budget at the very bright end of the LFs.

The simulations do not include catastrophic redshift failures ($\Delta z = z_{\text{phot}} - z_{\text{spec}} > 5\sigma$), that are found to amount to $\sim 1\%$ down to $I_{AB} = 22.5$, and $\sim 2\%$ down to $I_{AB} = 24$. Although a small fraction, catastrophic failures could have a significant effect in the poorly populated bright part of the LF. However, the typical redshift degeneracy observed for the “training” sample of galaxies with spectroscopic redshift is between $z \sim 0.2$ and $z \sim 2.8$ (see Feldmann et al. 2006), i.e., outside of the redshift range considered in this study. We also note that our conclusions are based on galaxies with observed magnitudes brighter than $I_{AB} = 21$; at these magnitudes our photometric redshifts are very accurate.

The main conclusion of our paper is based on the number density of galaxies brighter than $2.5L_*$, in the redshift range $0.6 < z \leq 0.8$. The main question to ask is whether the red ETGs galaxies brighter than $2.5L_*$ are really in the redshift range $0.6 < z \leq 0.8$, or have been scattered there because of photometric redshift errors. For 18 ETGs brighter than $2.5L_*$, spectroscopic redshfit is available from the current version of the zCOSMOS-bright (i.e., $I_{AB} \leq 22.5$) catalog (Lilly et al. 2007): 18/18 have spectroscopic redshift in the 0.6–0.8

range. This, therefore, demonstrate that the our result is robust against photometric redshift errors.

B. Comparison with redshift zero: 1813 SDSS galaxies

We use the set of artificial images created by Kampczyk et al. (2007) from a selected sample of SDSS galaxies in order to calibrate our results with the $z = 0$ Universe. The artificial images simulate how the local galaxies would be observed in the COSMOS survey at redshift $z = 0.7$. Details on the generation of these images are given in the original reference.

In brief, the SDSS galaxies were selected in the redshift range $z \in [0.015, 0.025]$ to be brighter than $M_B = -18.5$. The SDSS g -band images of the selected galaxies were transformed to F814W COSMOS ACS images at $z = 0.7$. At this redshift, the redshifted g band well matches the HST F814W passband; thus, the redshifting of the SDSS galaxies needs only to take care of the different pixel scales and point spread functions, and of cosmological surface brightness dimming. No galaxy size evolution was considered. The $z = 0.7$ simulated SDSS galaxies were then added into the COSMOS ACS images to reproduce the same circumstances of image crowding, noise, and so on. We expect the SDSS sample to be representative of the local galaxy population down to $M_B = -18.5$ since, overall, the photometric+spectroscopic SDSS data are mostly complete down to $r \sim 17.8$ (Strauss et al. 2002), i.e., well below the considered absolute magnitude cut that we applied.

The $z = 0.7$ simulated SDSS galaxies were analyzed with the same procedure used for the real COSMOS data. First, we run SExtractor to perform the detection and measure the I -band magnitude, position angle and elongation. For the detection we used the same SExtractor configuration parameters used to generate the COSMOS-catalog (Leauthaud et al. 2007). A fraction of 6% of the simulated galaxies was not detected, while a fraction of 0.1% was found with $I \gtrsim 24$, and therefore excluded from the sample. We then classified the galaxies using ZEST. Rest-frame properties such as $U - V$ colors, B -band absolute magnitudes, radii in kpc, were derived assuming that all galaxies were at redshift $z = 0.7$; the $U - V$ colors and M_V magnitudes were derived by logarithmic interpolation between the observed SDSS magnitudes (u , g , and r).

In Figure 12 we present the $U - V - M_V$ color-magnitude diagram (right panel) and the Kormendy diagram (left panel) for the simulated $z = 0.7$ SDSS galaxies. In particular, we show on the Kormendy diagram all galaxies classified as Type 1 or Type 2.0 with different colors according to the ZEBRA best-fits to their SEDs. As in Figure 1, red points represent

elliptical-galaxy SEDs, and blue points represent later photometric types. As expected, the SDSS morphologically-classified ellipticals are all consistent with the $z = 0$ Kormendy relation, as possible small-size faint interlopers are excluded from the sample by the imposed magnitude cut (see dotted line in the left panel of Figure 12, which shows the $I_{AB} = 24$ magnitude limit).

In the *right panel* of Figure 12 we show as gray points all SDSS galaxies in the original sample, and, highlighted in red, all galaxies with a ZEBRA elliptical-galaxy SED. The rest-frame colors were derived using the SDSS total magnitudes, and therefore represent the global galaxy color. As mentioned in Section 3.2.1, ETGs show color gradients with an average value of $d(U - V)/d(\log R) = -0.15$ (Scodreggio 2001). Due to this color gradient, the galaxy colors depend on the aperture size used for the photometric measurements; the colors are systematically bluer the larger the aperture. Since the average color gradient does not correlate with galaxy luminosity, the global effect of a large aperture is a blueing of the red-sequence relative to that derived using a smaller aperture. Assuming, for simplicity, that early-type galaxies in the local universe have a De Vaucouleur profile, and using the color gradients published by Scodreggio (2001), we estimate that the difference between the $U - V$ colors computed within 30% of the half-light radius and those calculated using total magnitudes amounts to ~ 0.1 magnitudes. In the Figure, the colors are corrected to account for the aperture corrections.

Assuming that the color-magnitude relation of $z = 0$ early-type galaxies can be interpreted as a pure metallicity sequence (Kodama et al. 1998; Bernardi et al. 2003a), with less luminous galaxies being more metal poor than more luminous galaxies, in Figure 12 we show the $U - V$ colors derived for single stellar population models of different metallicities formed at $z_f = 2$ (Bruzual & Charlot 2003). The colors of the models, together with the absolute V -band absolute magnitude, metallicity and mass of the galaxy are reported in Table 4.

We thank the anonymous referee for the careful reading of the manuscript, and the comments that helped to improve the presentation and discussion of our results. The HST COSMOS Treasury program was supported through NASA grant HST-GO-09822. We gratefully acknowledge the contributions of the entire COSMOS collaboration. More information on the COSMOS survey is available at <http://www.astro.caltech.edu/~cosmos>. We thank the NASA IPAC/IRSA staff for providing online archive and server capabilities for the COSMOS datasets. T. Lisker is acknowledged for helping with a preliminary reduction of a fraction of the ground-based near-infrared data. CS acknowledges support from the Swiss National Science Fondation.

Facilities: HST (ACS)

Table 4. Models of elliptical galaxies at $z = 0$ ($z_f = 2$).

M_V (mag) (1)	$U - V$ (mag) (2)	Z/Z_\odot (3)	M_* (M_\odot) (4)
-18.3	1.75	0.62	9.5×10^9
-19.9	1.81	0.79	4.4×10^{10}
-21.5	1.87	0.99	2.0×10^{11}
-23.4	1.93	1.26	1.2×10^{12}

Note. — The columns are: (1) V -band absolute magnitude; (2) $U - V$ rest-frame color, uncorrected for aperture effects; (3) stellar metallicity; and (4) total stellar mass.

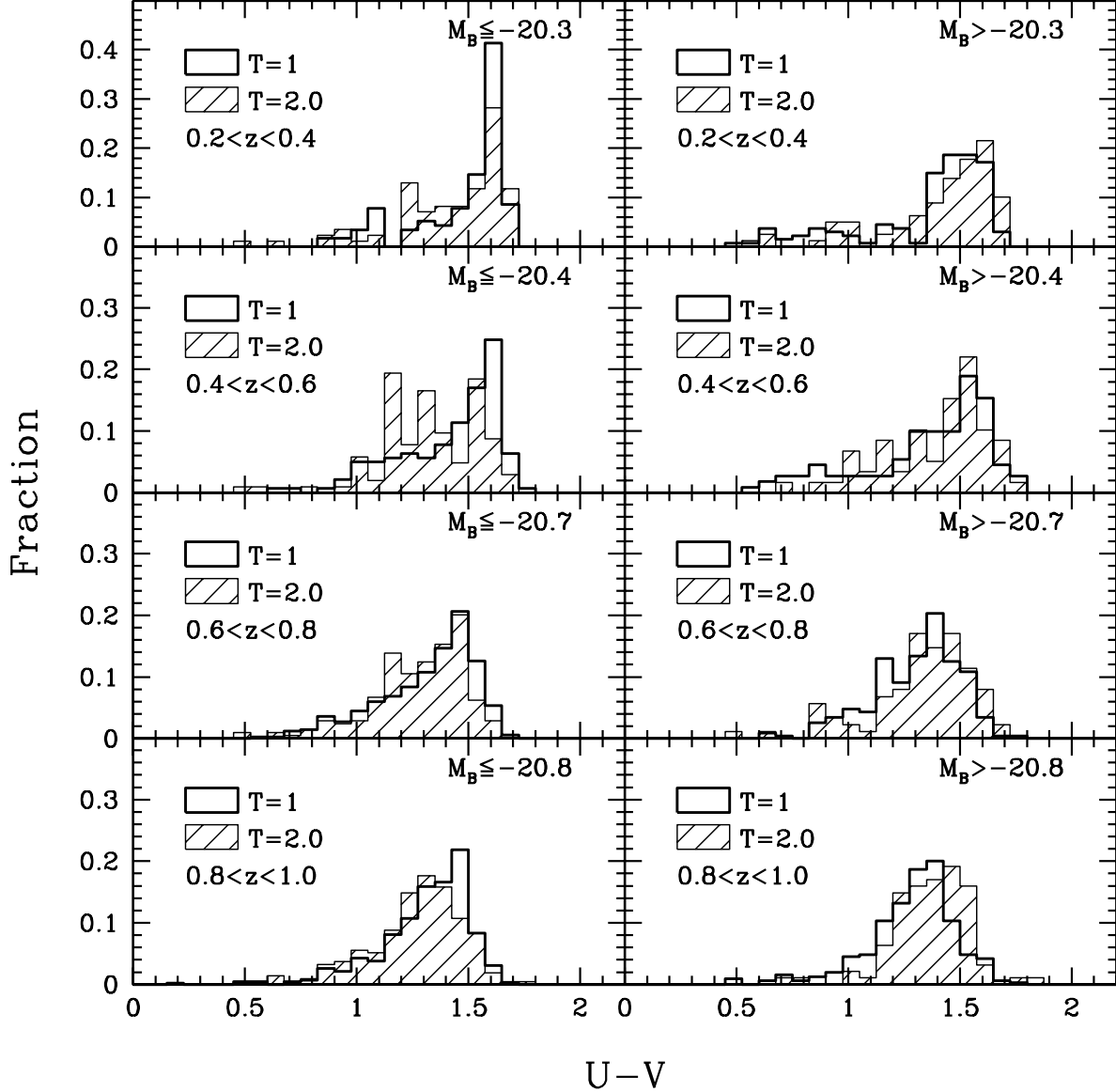


Fig. 6.— The distribution of rest-frame $U - V$ color for the Type 1 (early-type galaxies; solid histograms) and Type 2.0 (disk galaxies; dashed histograms) galaxies that pass the Kormendy-relation test, and are thus kept in the final morphologically-selected sample of ETGs. Left and right panels are for galaxies brighter and fainter than M_B^* , respectively. The values of M_B^* are derived from the Schechter fits to the LFs of the morphologically-selected sample (see text), and are given in the upper-right corners of the diagrams.

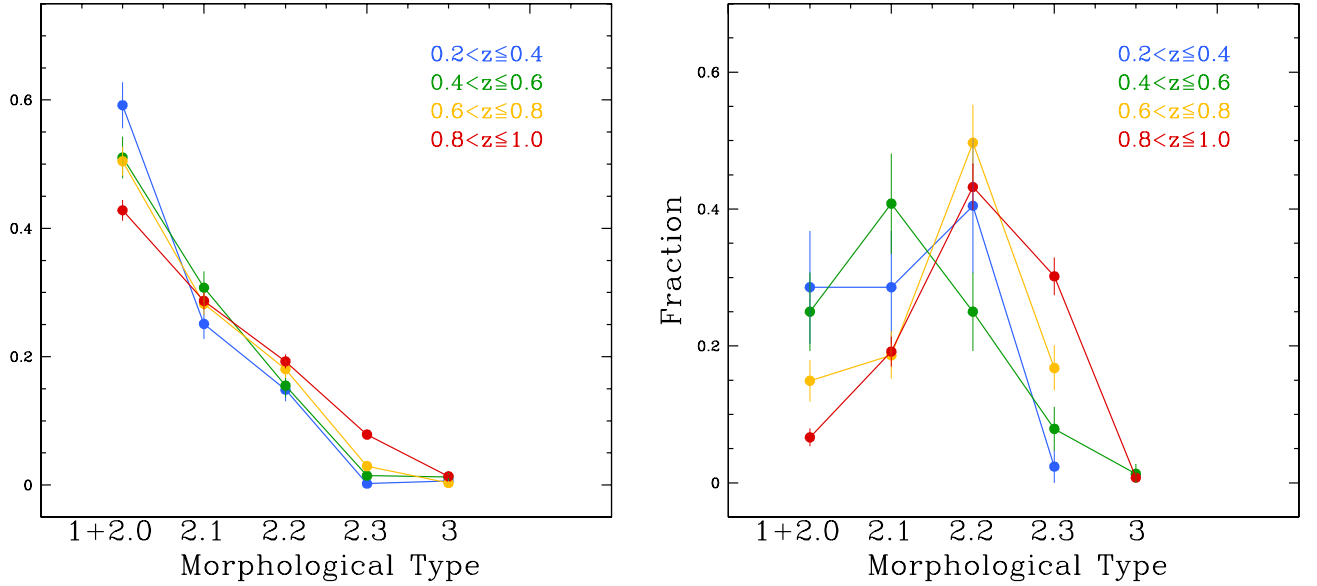


Fig. 7.— Left panel: Fraction of photometrically-selected early-type galaxies with different ZEST morphological types (Type 1 + 2.0 = morphological early-type; 2.1 to 2.3 = disk dominated spirals; 3 =irregulars). In the right panel we show the results for the photometrically-selected galaxies which do not pass the Kormendy-test. To make the comparison among different redshift meaningful, we consider (in both panels) only galaxies brighter than $M_B = -18.16, -18.44, -18.72,$ and -19 at $z = 0.3, 0.5, 0.7,$ and $0.9,$ respectively. Results for different redshift bins are shown in different colors.

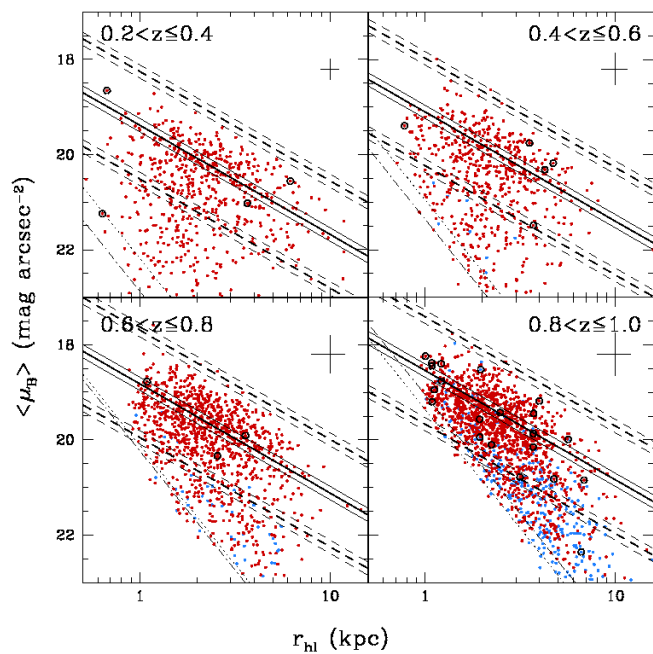


Fig. 8.— The Kormendy diagram for the sample of photometrically-selected early-type galaxies of Section 3.2. Large black circles identify galaxies with irregular morphological classification (ZEST Type 3). Red dots are galaxies with SEDs best fitted by ZEBRA with an elliptical-galaxy template; blue dots identify objects which are fitted by ZEBRA with a late-type galaxy template.

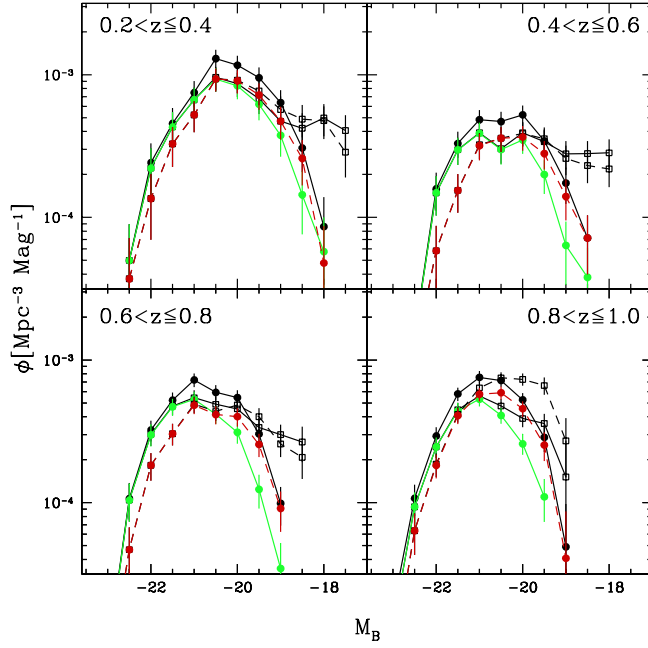


Fig. 9.— LFs derived using the $1/V_{max}$ formalism and the ZEBRA Maximum Likelihood photometric redshifts. Green, red and black show respectively the morphologically-, photometrically-selected, and combined sample of COSMOS early-type galaxies. The black open symbols and lines show the LFs derived without applying the Kormendy selection cuts (solid: morphological sample; dashed: photometric sample). The error bars indicate Poisson errors only. Note that the relatively high normalization factor in the lowest redshift bin is due to the well known overdensity in the central region of the COSMOS field.

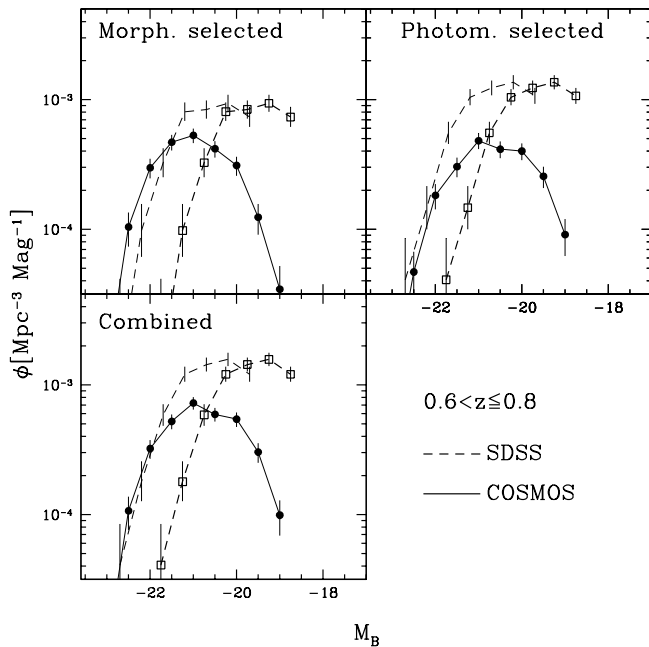


Fig. 10.— Comparison of the SDSS LFs, redshifted to $z = 0.7$ (empty symbols, dashed lines), and the $0.6 < z \leq 0.8$ COSMOS LFs (filled symbols, solid lines), for the morphologically-selected and photometrically-selected samples, and for the combined sample of ETGs. The SDSS LFs are shown also brightened by 0.95 magnitude, i.e., the amount consistent with the evolution of the red sequence in the rest-frame $U - V$ vs. M_V color-magnitude diagram (thin dashed curves).

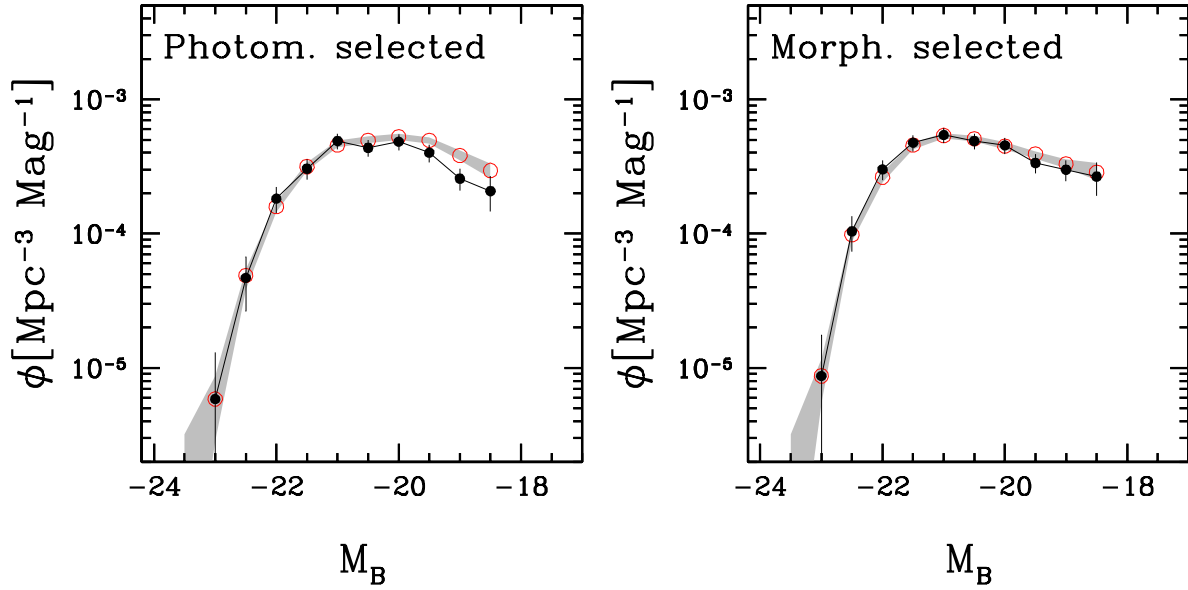


Fig. 11.— Results of the simulations performed to assess the impact of the photometric redshift errors in the calculation of the LFs in the redshift range $0.6 < z \leq 0.8$. The solid circles with errorbars represent the LF of the original COSMOS catalog used to generate the 100 simulated datasets. On the right and left panel we show, respectively, the results for the photometrically- and morphologically-selected samples of early type galaxies. The grey area indicates the 16th-to 84th percentiles of the distributions -in each magnitude bin- of the 100 realization of the COSMOS catalog.

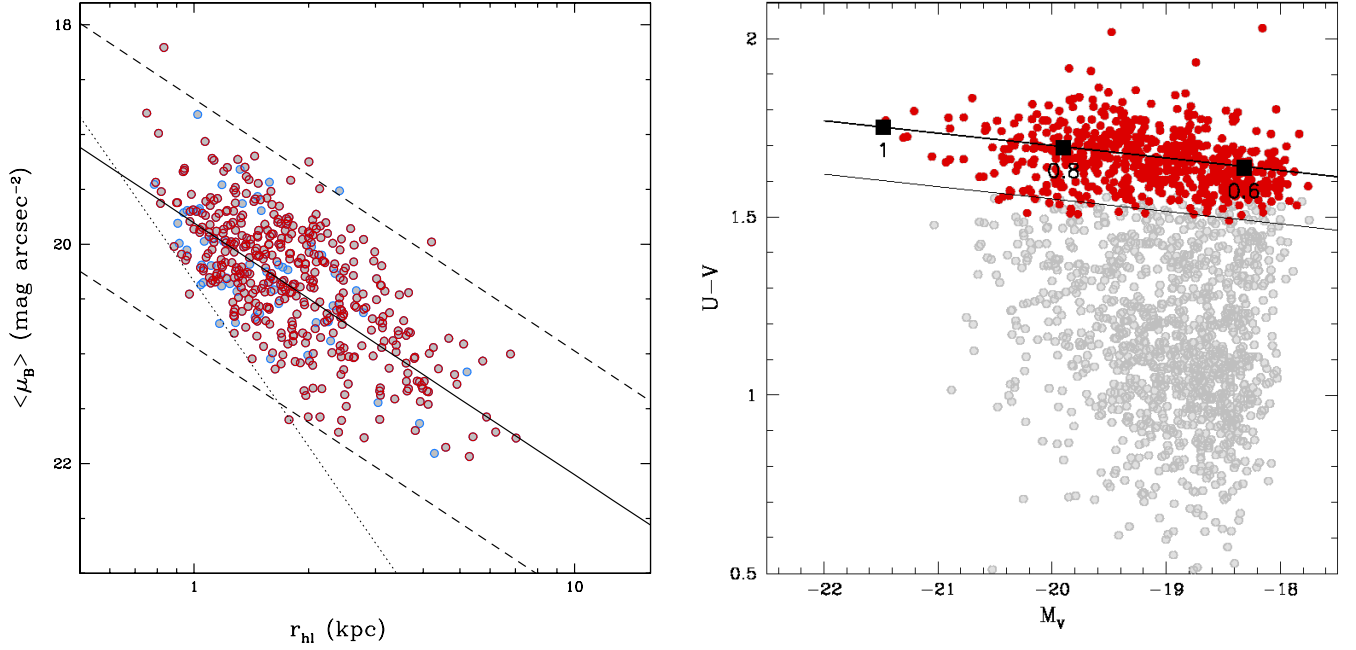


Fig. 12.— Left panel: Kormendy diagram for all SDSS galaxies classified as Type 1 (early-type) and Type 2.0 (bulge-dominated disk galaxies) with ZEST. Points are color-coded according to their ZEBRA photometric class: red points correspond to galaxies with ZEBRA elliptical-galaxy fits, and blue points are used for galaxies with SEDs fitted by ZEBRA with later spectral types. The solid black line shows the best linear fit derived for Coma cluster galaxies (Jørgensen, Franx & Kjærgaard 1995). Dashed lines are $2 \times \text{rms}$ away from the COMA best-fit line. The dotted line shows the magnitude limit applied to select the SDSS sample. Right panel: Rest-frame $U-V$ versus the absolute V magnitude for all SDSS galaxies (gray circles). In red are highlighted galaxies with an SED best-fitted by ZEBRA with an elliptical-galaxy template. The large black squares show the aperture-corrected colors and magnitudes for a set of single stellar population models with different metallicities (from $0.6Z_{\odot}$ to Z_{\odot}).